General Disclaimer

One or more of the Following Statements may affect this Document

- This document has been reproduced from the best copy furnished by the organizational source. It is being released in the interest of making available as much information as possible.

- This document may contain data, which exceeds the sheet parameters. It was furnished in this condition by the organizational source and is the best copy available.

- This document may contain tone-on-tone or color graphs, charts and/or pictures, which have been reproduced in black and white.

- This document is paginated as submitted by the original source.

- Portions of this document are not fully legible due to the historical nature of some of the material. However, it is the best reproduction available from the original submission.

NAS CR-135187
TRW ER-7926

STRAIN PARTITIONING OF THREE ALLOYS IN ULTRAHIGH VACUUM USING THE STEP STRESS METHOD

FINAL REPORT

APRIL 1977

prepared for

NATIONAL AERONAUTICS AND SPACE ADMINISTRATION

UNDER CONTRACT NAS-3-20103

TRW MATERIALS TECHNOLOGY LABORATORIES
CLEVELAND, OHIO

FOREWORD

The work described in this report was performed in the Materials Technology Laboratory of TRW Inc. under sponsorship of the National Aeronautics and Space Administration; Contract NAS 3-20103. The program was administered for TRW by Mr. J. A. Alexander, Program Manager. The Principal Investigator was Dr. C. S. Kortovich, with technical assistance provided by Mr. J. W. Sweeney. The NASA Technical Manager was Dr. G. R. Halford.

Prepared by: C. S. Kortovich
C. S. Kortovich
Section Manager

Approved by: J. A. Alexander
J. A. Alexander
Manager
Materials Research Dept.

TABLE OF CONTENTS

I INTRODUCTION

The concept of Strainrange Partitioning as a method to analyze complex creep-fatigue problems was introduced in 1971 (1). Since this time the method has exhibited a capability of unifying this complex field. In particular, the method can treat problems related to fatigue data obtained under thermal-mechanical strain-cycling involving the simultaneous independent variation of both strain and temperature (2,3). Thus, complex thermal-mechanical problems can be analyzed on the basis of true variation of service conditions, rather than requiring simplified assumptions that may miss some of the essence of the problem.

Within the framework of this method, cyclic damage is contributed by each of the four generic partitioned strainranges in proportion to the amount of each present within a cycle. Once the basic strainrange components that underlie the partitioning concept have been determined, a suitable damage rule can then be applied to determine the life more precisely. In most general types of thermal-mechanical cycling where loading is usually gradual, both creep and plastic types of strain may occur within the same time increment, and it becomes important to separate them so that a partitioning analysis can be made.

The present study was undertaken in order to further characterize the partitioned strainrange behavior of three alloys including ASTAR 811C, 304 stainless steel and A-286 by providing additional data for evaluation of the strainrange partitioning concept. This objective was accomplished by testing specimens utilizing the "step stress" method of experimental strain separation (4,5). This procedure provided results and data which may be used to enable the partitioning of the inelastic strainranges previously established during the high temperature, low cycle fatigue testing of the three alloys as reported in NASA CR-121001 and CR-134524 prepared by TRW Inc.

II EXPERIMENTAL PROCEDURES

The three alloys studied in the present program included ASTAR 811C, 304 stainless steel and A-286. Tests were conducted on solid hourglass specimens provided by the sponsor and shown schematically in Figure 1. Equipment and procedures used for the vacuum thermal fatigue tests in this program have been described in detail in previous reports (6,7). Briefly, the test apparatus was designed to perform completely reversed push-pull fatigue tests on hourglass specimens using independently programmable temperature and strain control. Temperature was programmed using a thyratron-controlled 50 KV AC transformer for direct resistance heating of the specimen, while diametral strain was controlled directly using an LVDT type extensometer coupled to a programmable closed loop electrohydraulic servo system. The measured specimen diameter was compensated electronically for thermal expansion so that net mechanical strain was controlled directly. Load, diameter and temperature were recorded continuously, with load-diameter hysteresis loops being obtained at periodic intervals during each test.

The test program involved both isothermal and thermal-mechanical strain cycling for the purpose of separating the creep and plastic strain components of the inelastic strains that develop during cycling. All testing was conducted at a frequency of 0.0065 Hz in an ultrahigh vacuum environment below 10^{-7} torr. The specific conditions of temperature and strain cycling for each test are listed in Table 1. It will be noted that a number of these tests duplicate conditions tested previously at TRW as reported in NASA CR-121001 and CR-134524 written by TRW Inc. (6,7). For identification purposes the original test numbers for these particular tests have also been included in Table 1. A schematic representation of the five basic types of thermal-mechanical cycles applied in this study are presented in Figure 2.

The "step-stress" method of experimental strain separation was utilized to study the partitioned strainrange behavior of the ASTAR 811C, 304 stainless steel and A-286 alloys. This technique has been described previously (1-4). Briefly, within the framework of this separation method, the component of steady-state creep for the entire period of the time interval considered in a thermal-mechanical strain cycling problem is taken as the "creep" strain for use in strainrange partitioning analysis. All the remaining inelastic strain, whether instantaneous or whether occurring as primary creep, is taken to be "plasticity." The partitioning procedure is to halt, temporarily, the temperature and strain programmers at a selected point in a stabilized hysterisis loop. The servo-controller is then switched from strain to load control and the stress and temperature are held constant at the stabilized values associated with the selected point while creep strain is measured as a function of time. This condition is held until a reasonably linear creep rate is established. This is taken as an approximation to the steady state creep condition. The controller is then switched back to strain control and the strain and temperature programs are resumed. A series of step-stress levels are thus

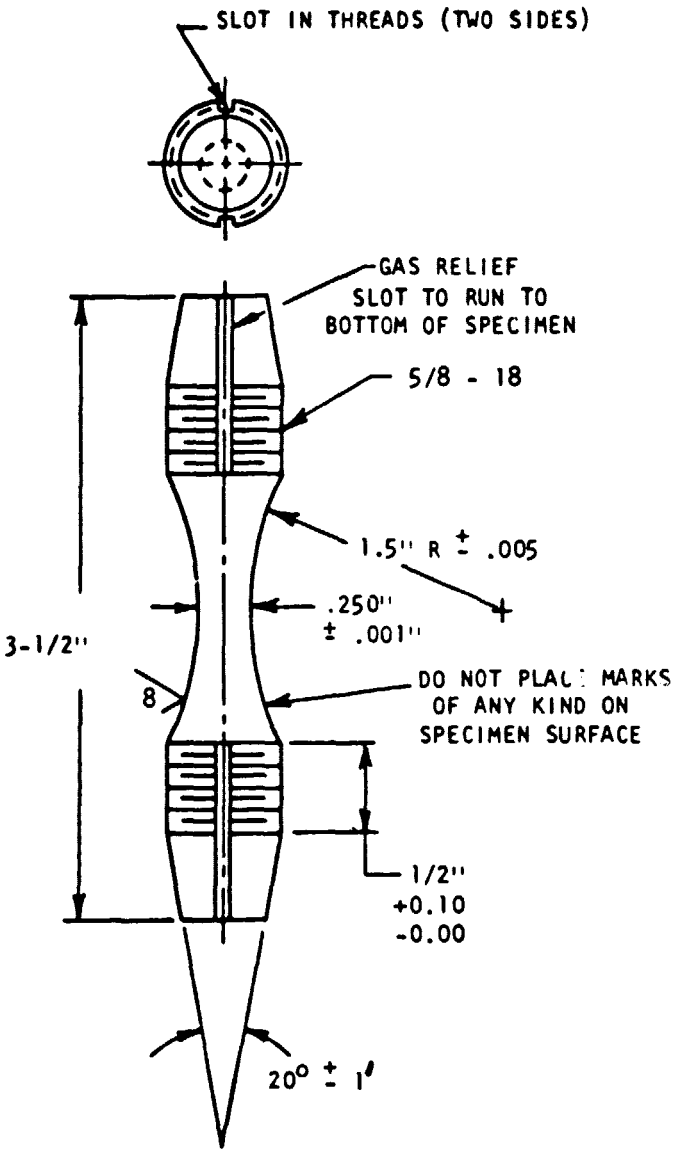

Figure 1. Test Specimen for Thermal Fatigue Testing.

Table I

Conditions of Temperature and Strain Cycling for Fatigue Tests Conducted in the Present Program

Alloy	Specimen Number	Test Condition	Previous Specimen Number	Previous Report
ASTAR 811C	A1D	ISOT 2100°F (1149°C)	A1	NASA CR-121001 (6)
"	A15D	TCIP 2100°F (1149°C) - 400°F (204°C)	A15	" " "
"	A21D	TCOP 400°F (204°C) - 2100°F (1149°C)	A21	" " "
"	A49D	TCIPS 2100°F (1149°C) - 400°F (204°C)	A49	" " "
304 Stainless	A21A	ISOT 1200°F (649°C)	A4A	NASA CR-134524 (7)
" "	A24A	TCIP 1200°F (649°C) - 600°F (316°C)	(*)	-
" "	A25A	TCOP 600°F (316°C) - 1200°F (649°C)	(*)	-
" "	A22A	TCIPS 1200°F (649°C) - 600°F (316°C)	A7A	NASA CR-134524 (7)
" "	A23A	TCOPS 600°F (316°C) - 1200°F (649°C)	A11A	" " "
A-286	L57	ISOT 1100°F (593°C)	L44	NASA CR-134534 (7)
"	L61	TCIP 1100°F (593°C) - 600°F (316°C)	(*)	NASA CR-134524 (7)
"	L62	TCOP 600°F (316°C) - 1100°F (593°C)	(*)	-
"	L58	TCIPS 1100°F (593°C) - 600°F (316°C)	L50	NASA CR-134524 (7)
"	L59	TCOPS 600°F (316°C) - 1100°F (593°C)	L51	" " "

(*) These Tests will be conducted to failure.

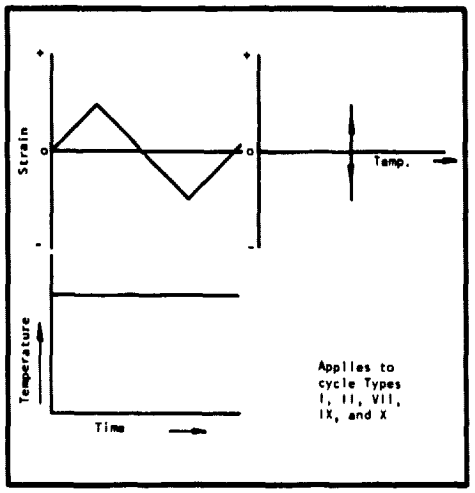

(a) Isothermal

Note: All strains shown represent Net mechanical strain, with thermal expansion subtracted out.

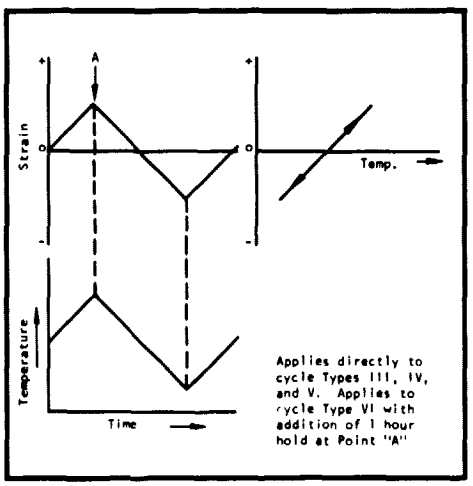

(b) TCIP

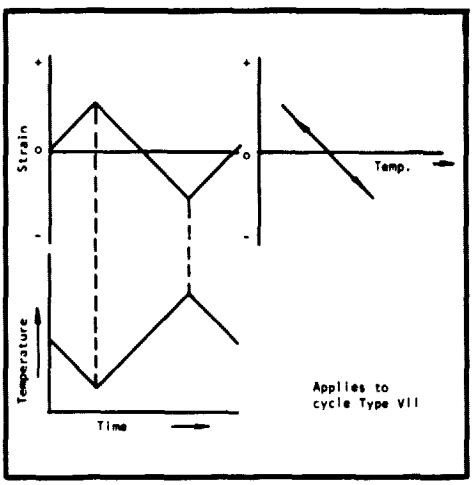

(c) TCOP

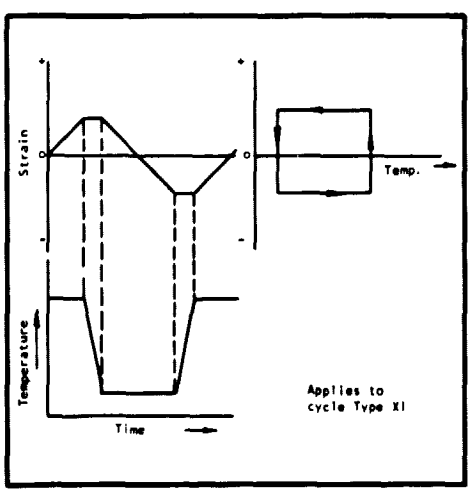

(d) TCIPS

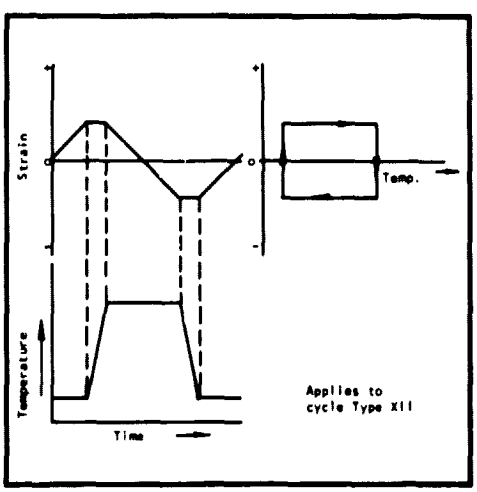

(e) TCOPS

Figure 2. Schematic Representation of the Five Basic Types of Thermal-Mechanical Cycles Applied in This Study.

investigated both in the tensile and compressive portions of the hysteresis loop. A plot of the steady-state creep rate versus time within the thermal-mechanical cycle that each stress and temperature was encountered is then constructed. By integrating the area under this curve, the amounts of tensile and compressive steady-state creep strain can be determined. Areas above the horizontal axis represent tensile creep, those below the horizontal axis represent compressive creep.

III RESULTS AND DISCUSSION

A. Test Results

The dynamic stress-strain response (hysteresis loops) for all the fatigue tests conducted in this program are presented in Appendix A along with each typical load-time trace and strain-time trace for the cyclically stabilized condition. The isothermal loops were basically symmetrical for all three materials. Assymetric hysteresis loops were developed with all four types of thermal fatigue cycles. This assymetry was caused by the difference in flow stress at the different temperature levels. In-phase cycling generated loops having a net compressive stress, while out-of-phase cycling caused a mean tensile stress to be developed.

The results of the fourteen fatigue tests conducted in this program are presented in Table II. For clarity of presentation, these results have been grouped according to the various alloys tested (A-286, 304 stainless steel and ASTAR 811C). The present study was undertaken in order to determine the partitioned strainrange behavior of these alloys and to provide additional data for evaluation of the strainrange partitioning concept. In order to accomplish these objectives, a number of the tests were conducted duplicating conditions tested previously at TRW (6,7). These particular tests were not conducted to failure in the present program and are specifically identified in Table II.

The data presented in Table II include axial total strainrange, axial elastic strainrange, axial inelastic strainrange, axial stress range and number of cycles to failure (complete specimen separation) for those tests continued to failure. The step stress method of strainrange partitioning was utilized to accomplish partitioning of the inelastic strainranges. Within the framework of this method, a plot of the steady state creep rate versus time within a thermal mechanical cycle that each stress and temperature was encountered was constructed. By integrating the area under this curve, the amounts of tensile and compressive steady state creep strain were determined. The component of steady state creep for the entire period of the time interval considered was taken as the "creep" strain for use in strainrange partitioning analysis. The various plots of steady state creep rate versus time for the thermal-mechanical cycles applied in this study are shown in Figures 3-16.

In order to illustrate this strainrange partioning method as applied to a complicated thermal mechanical problem, consider the plot of steady state creep rate versus time during in-phase thermal-mechanical strain cycling 2100°F (1149°C) 400°F (204°C) applied to ASTAR 811C (Specimen A15D) shown in Figure 4. Areas above the horizontal axis represent tensile creep, those below the horizontal axis represent compressive creep. In this example the compressive steady state creep strain is 0.00005. Since the compressive inelastic strain is 0.02560, the compressive plastic strain is 0.02555. Similarly, the tensile creep strain as determined from Figure 4 is 0.00018. Since the tensile inelastic strain is also equal to 0.02560, the tensile plastic strain is 0.02542. Hence, the partitioned strainranges are:

$$\Delta\varepsilon_{pp} = 0.02542, \quad \Delta\varepsilon_{cc} = 0.00005, \quad \Delta\varepsilon_{cp} = 0.00013$$

Table II

Summary of Fatigue Results for Strainrange Partitioning Tests Conducted on ASTAR 811C, 304 Stainless and A-286

Alloy	Specimen Number	Test Condition	Axial Strainrange			Axial Partitioned Inelastic Strainranges				Axial Stress Range						Cycles to Failure
										Maximum Stress		Minimum Stress		Range		
			Total	Elastic	Inelastic	$\Delta\varepsilon_{pp}$	$\Delta\varepsilon_{cc}$	$\Delta\varepsilon_{cp}$	$\Delta\varepsilon_{pc}$	ksi	MPa	ksi	MPa	ksi	MPa	
ASTAR 811C	A1D	ISOT 2100°F(1149°C)	0.02433	0.00345	0.02088	0.02074	0.00014	-	-	45.2	311.7	38.3	264.1	83.5	575.7	
ASTAR 811C	A15D	TCIP 2100°F(1149°C)⇌ 400°F(204°C)	0.03082	0.00522	0.02560	0.02542	0.00005	0.00013	-	80.1	552.3	90.6	624.6	170.7	1176.8	
ASTAR 811C	A21D	TCOP 400°F(204°C)⇌ 2100°F(1149°C)	0.02543	0.00471	0.02063	0.02048	0.00009	-	0.00006	77.8	536.4	59.0	406.8	136.8	943.2	
ASTAR 811C	A49D	TCIPS 2100°F(1149°C)⇌ 400°F(204°C)	0.02345	0.00508	0.01837	0.01826	-	0.00011	-	65.5	451.6	69.7	480.5	135.2	932.2	
304 Stainless	A21A	ISOT 1200°F(649°C)	0.02359	0.00277	0.02082	0.02068	0.00014	-	-	41.2	284.1	36.4	251.0	77.6	535.0	
304 Stainless	A24A	TCIP 1200°F(649°C)⇌ 600°F(316°C)	0.01744	0.00352	0.01392	0.01390	0.00001	0.00001	-	50.0	344.7	48.6	335.0	98.6	679.9	260
304 Stainless	A25A	TCOP 600°F(316°C)⇌ 1200°F(649°C)	0.02880	0.00332	0.02548	0.02535	0.0001	-	0.00012	53.7	370.2	39.3	271.0	93.3	641.2	703
304 Stainless	A22A	TCIPS 1200°F(649°C)⇌ 600°F(316°C)	0.02624	0.00312	0.02312	0.02292	-	0.00020	-	42.2	291.0	45.3	312.4	87.5	603.2	
304 Stainless	A23A	TCOPS 600°F(316°C)⇌ 1200°F(649°C)	0.02309	0.00336	0.01972	0.01956	-	-	0.00016	54.1	373.0	39.9	275.1	94.0	648.1	
A-286	L57	ISOT 1100°F(593°C)	0.02502	0.00762	0.01740	0.01729	0.00011	-	-	86.6	597.0	88.7	611.5	175.3	1209.1	
A-286	L61	TCIP 1100°F(59[illegible]⇌ 600°F(316°C)	0.02535	0.01120	0.01415	0.01408	0.00007	0.00002	-	145.5	1003.1	128.2	883.9	273.7	1887.8	201
A-286	L62	TCOP 600°F(316°C)⇌ 1100°F(593°C)	0.03006	0.01150	0.01856	0.01841	0.00005	-	0.00010	171.5	1182.4	112.6	776.3	284.1	1960.7	356
A-286	L58	TCIPS 1100°F(593°C)⇌ 600°F(316°C)	0.03439	0.01299	0.0214	0.02123	-	0.00017	-	169.3	1167.1	155.5	1072.4	324.8	2245.5	
A-286	L59	TCOPS 600°F(316°C)⇌ 1100°F(593°C)	0.02740	0.01174	0.01566	0.01558	-	-	0.00008	149.4	1029.8	139.0	958.4	288.4	1990.8	

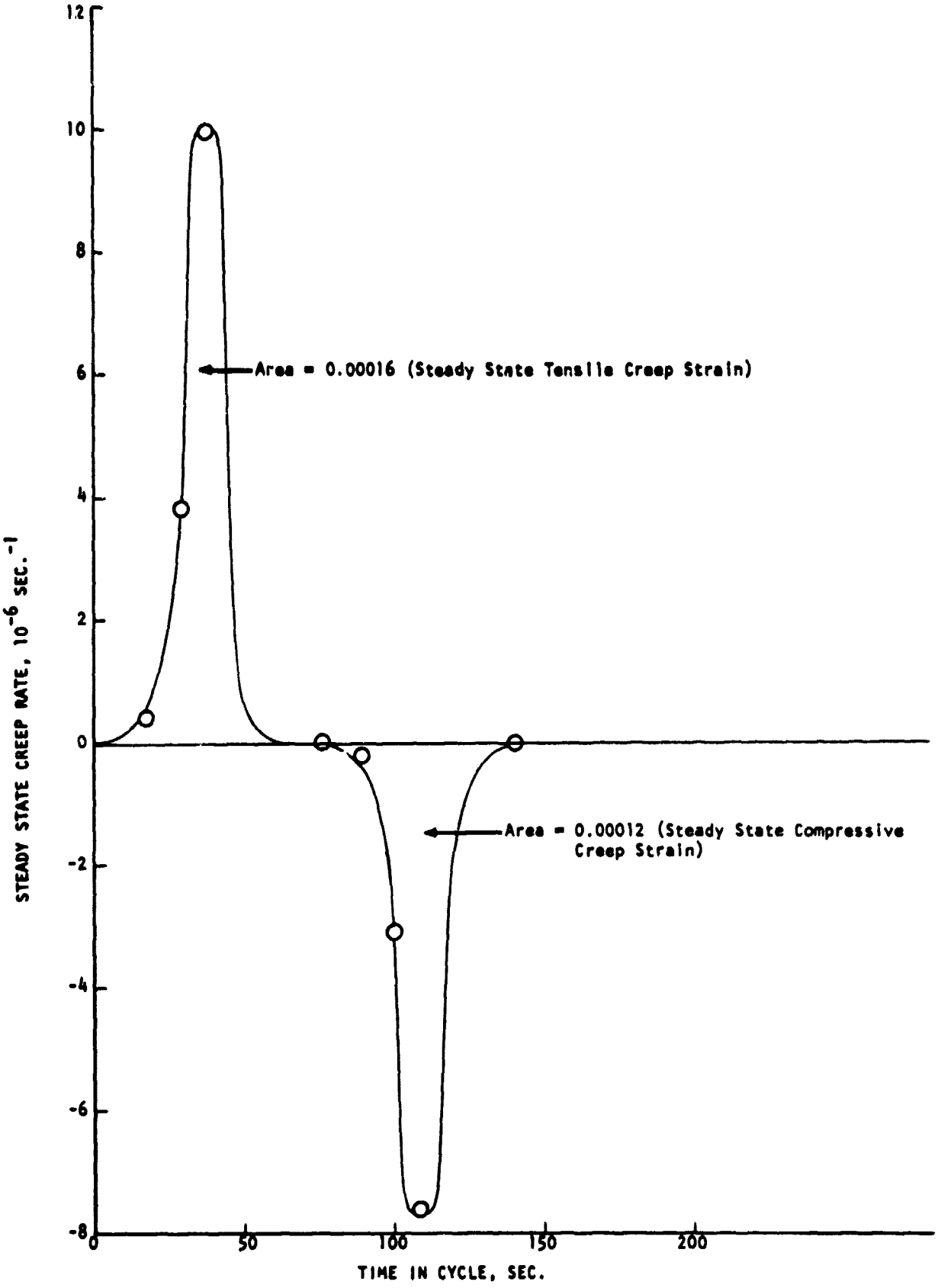

Figure 3. Accumulation of Tensile and Compressive Steady State Creep Strain During Isothermal-Mechanical Strain Cycle, 2100°F (1149°C), Applied to ASTAR 811C (Specimen A1D).

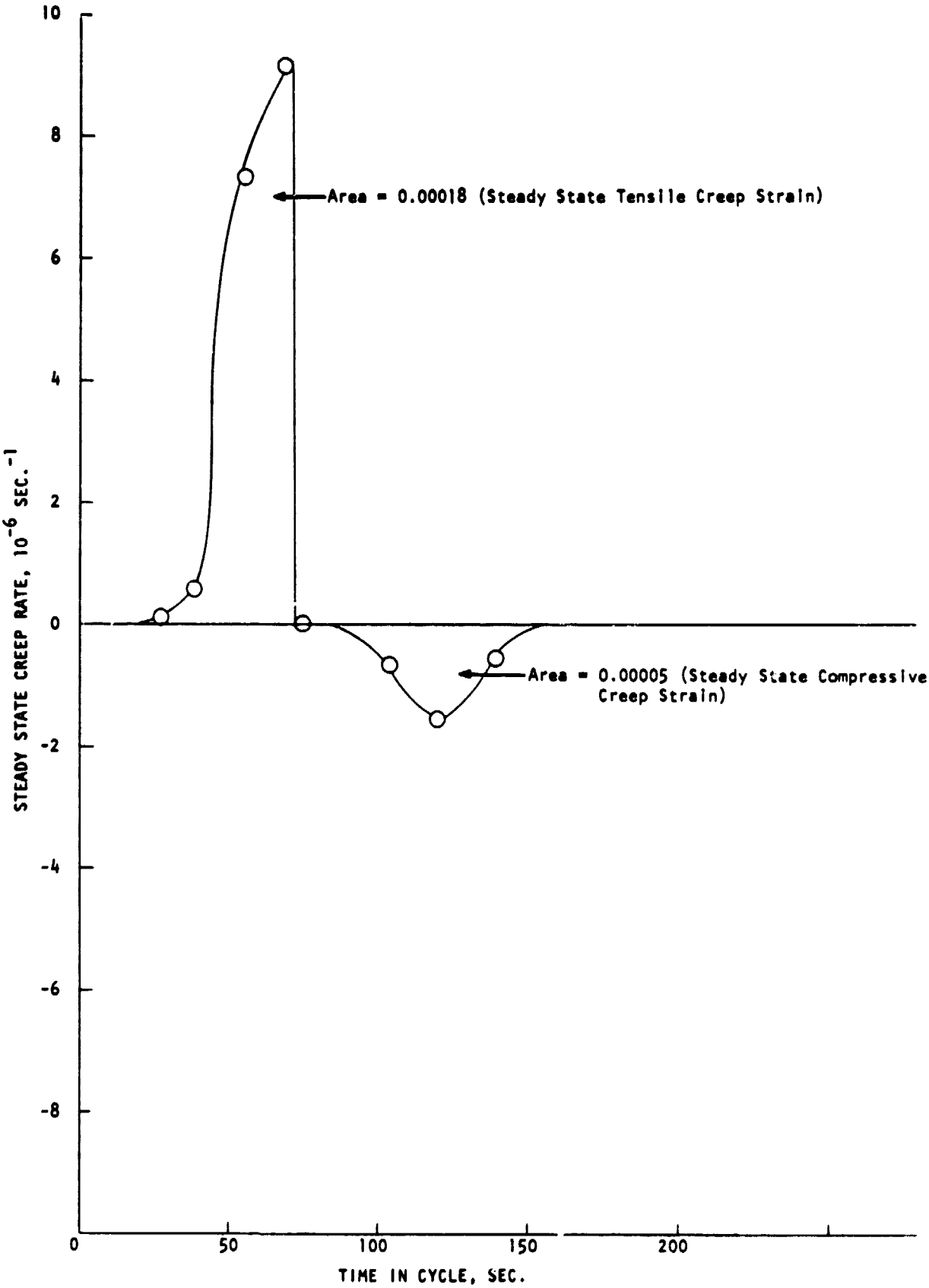

Figure 4. Accumulation of Tensile and Compressive Steady State Creep Strain During In-Phase Thermal-Mechanical Strain Cycle, 2100°F (1149°C)⇌400°F (204°C), Applied to ASTAR 811C (Specimen A15D).

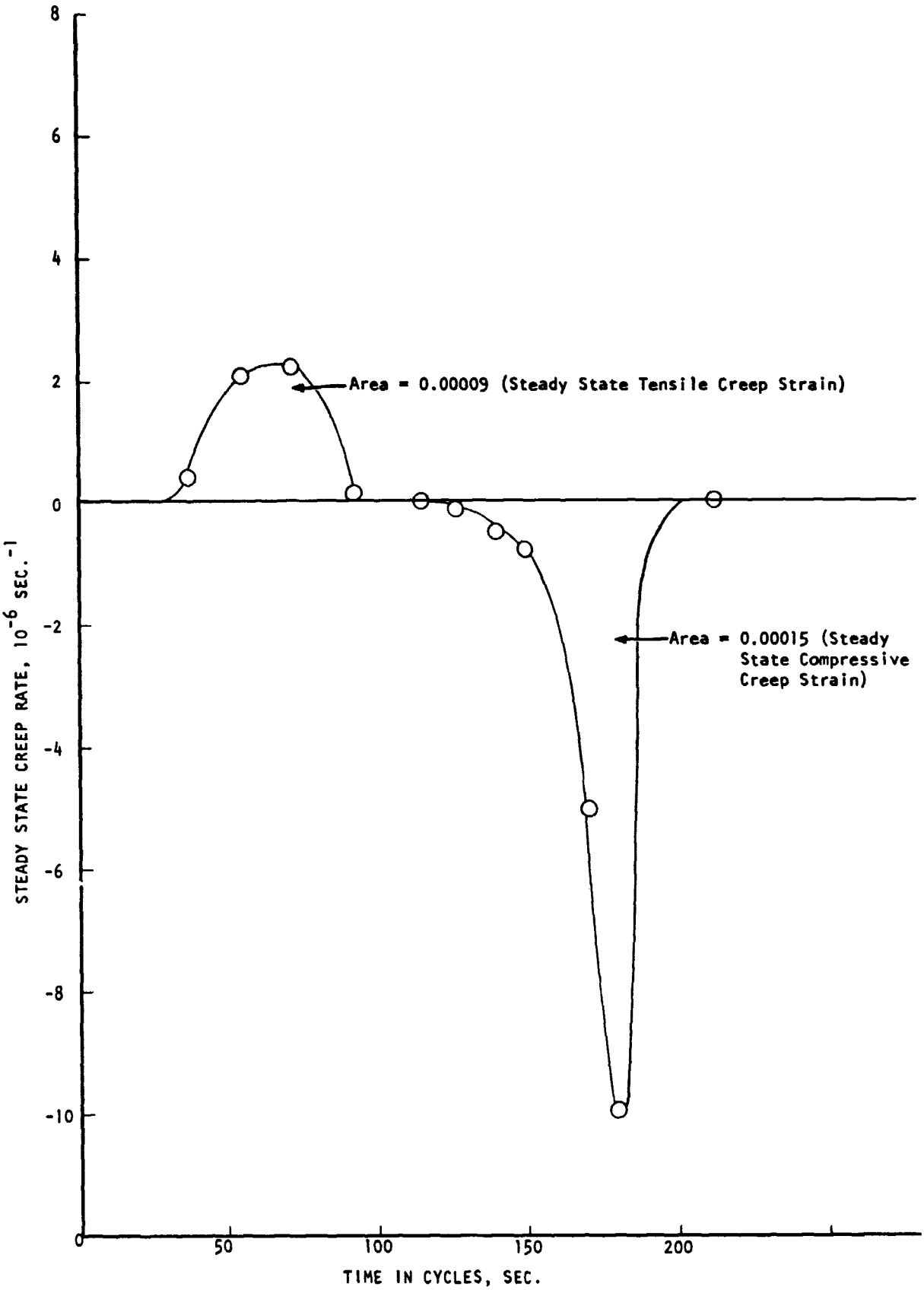

Figure 5. Accumulation of Tensile and Compressive Steady State Creep Strain During Out-of-Phase Thermal-Mechanical Strain Cycle, 400°F (204°C) $\rightleftharpoons$ 2100°F (1149°C), Applied to ASTAR 811C (Specimen A21D).

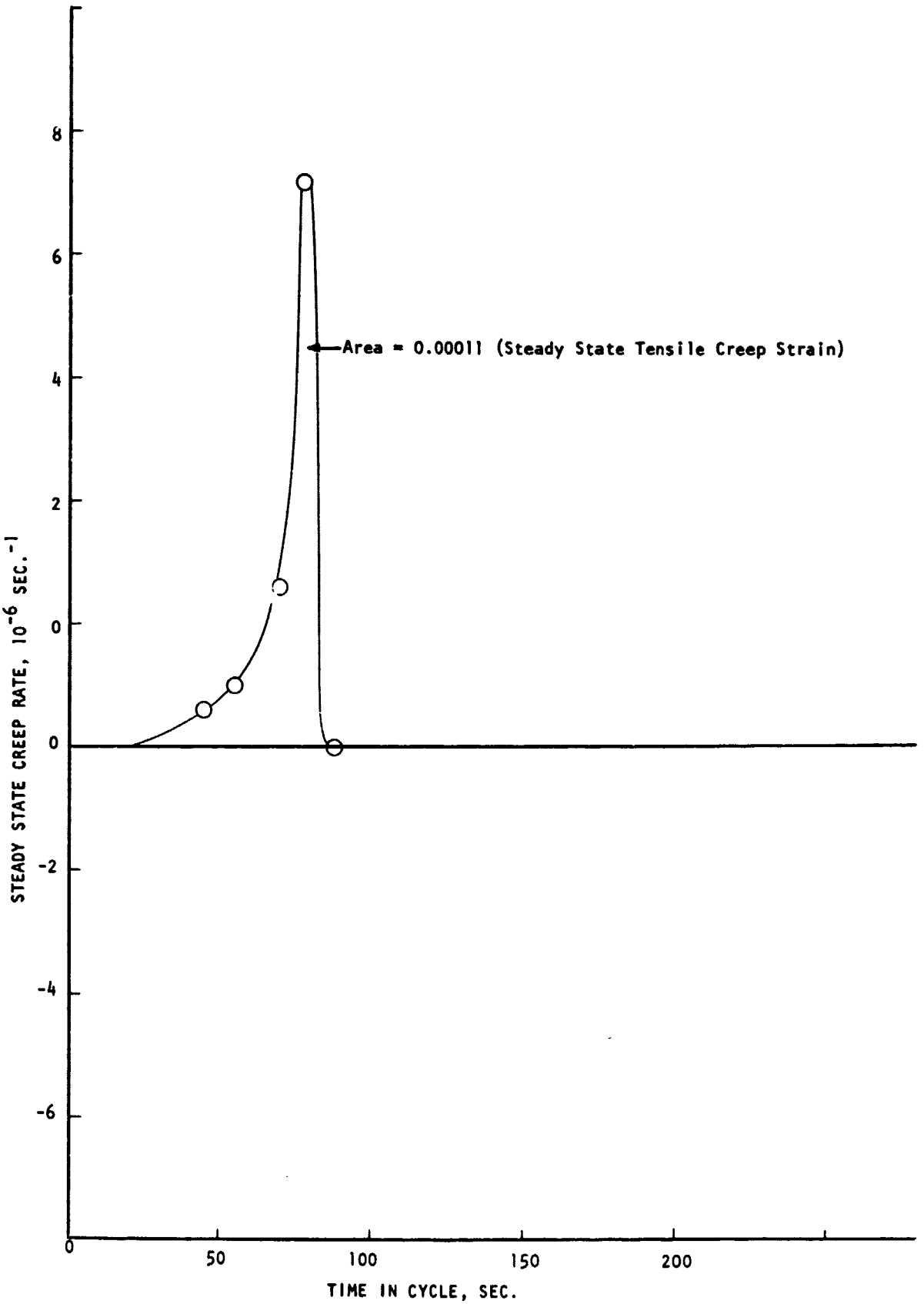

Figure 6. Accumulation of Tensile Steady State Creep Strain During In-Phase Square-Wave, Thermal-Mechanical, Strain Cycle, 2100°F (1149°C) ⇌ 400°F (204°C), Applied to ASTAR 811C (Specimen A49D).

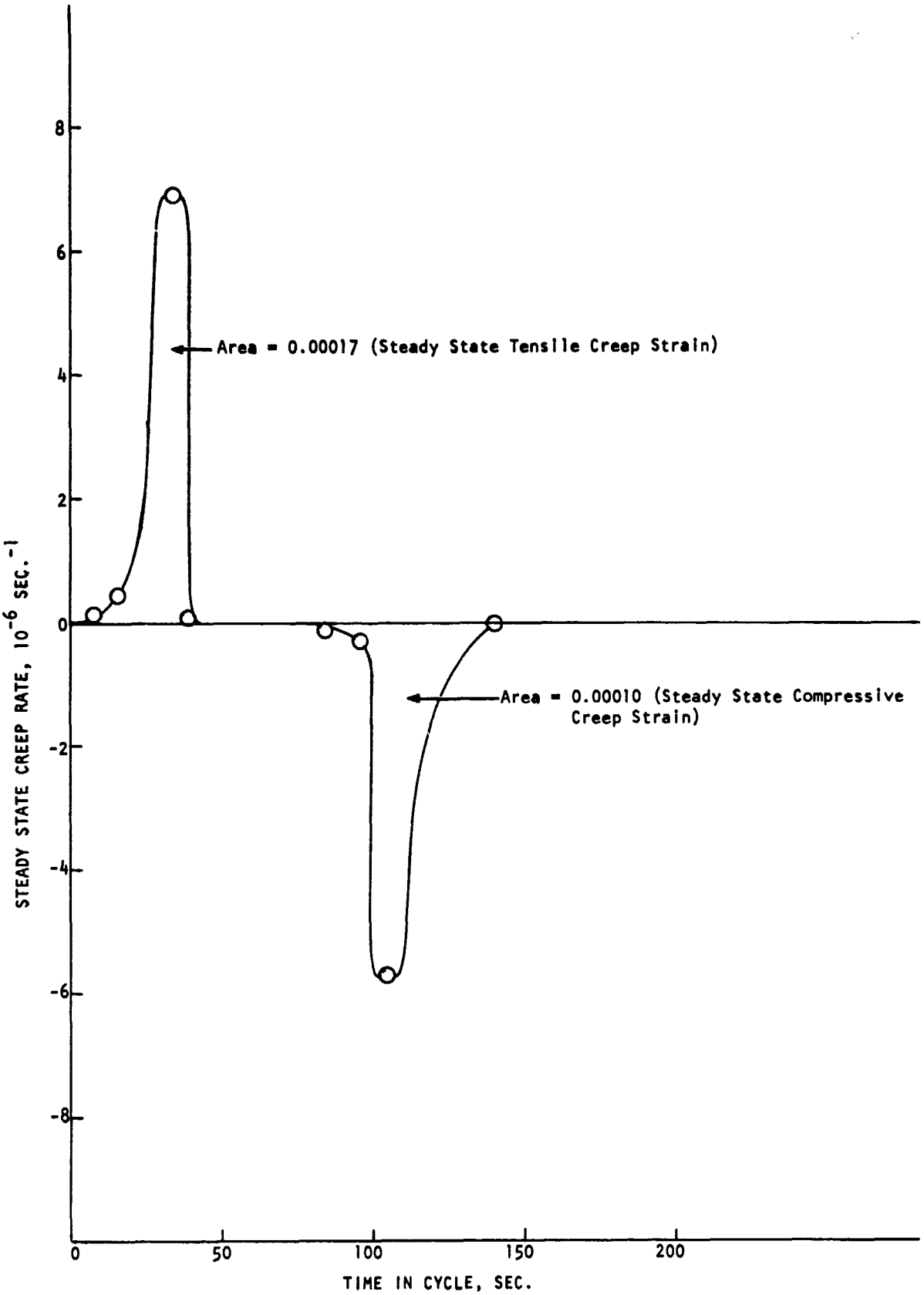

Figure 7. Accumulation of Tensile and Compressive Steady State Creep Strain During Isothermal-Mechanical Strain Cycle, 1200°F (649°C), Applied to 304 Stainless (Specimen A21A).

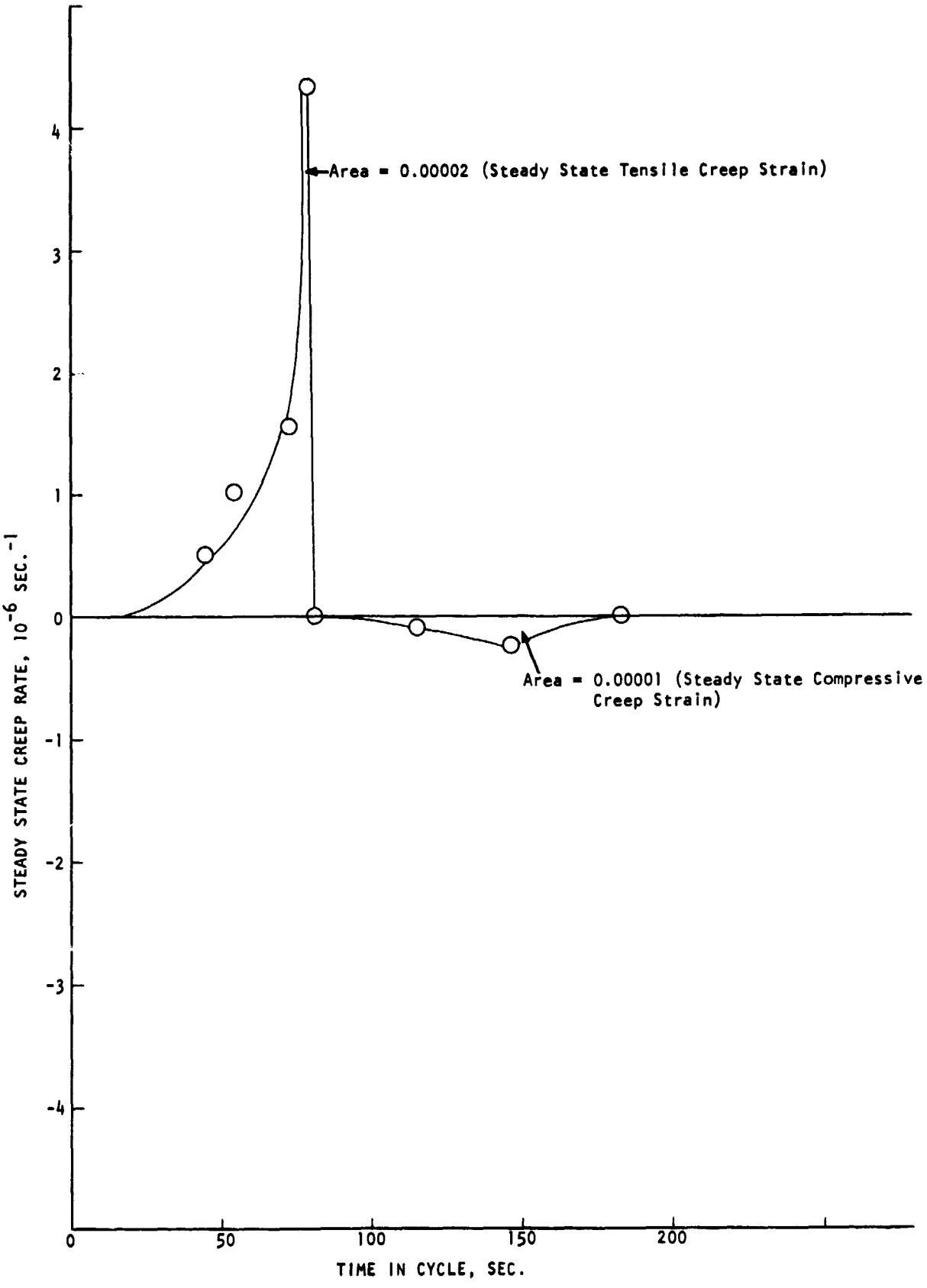

Figure 8. Accumulation of Tensile and Compressive Steady State Creep Strain During In-Phase, Thermal-Mechanical Strain Cycle, 1200°F (649°C) ⇌ 600°F (316°C), Applied to 304 Stainless (Specimen A24A).

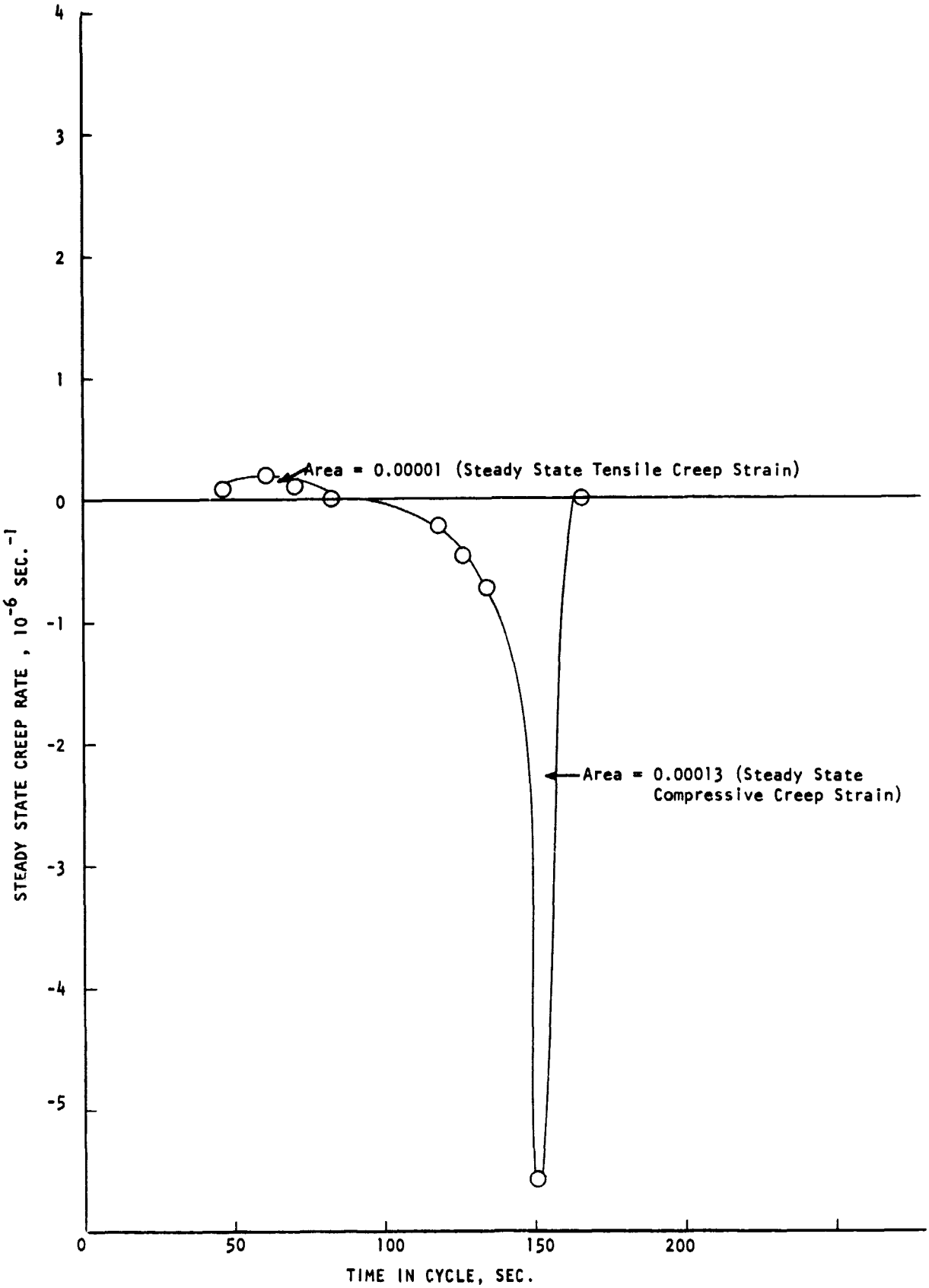

Figure 9. Accumulation of Tensile and Compressive Steady State Creep Strain During Out-of-Phase, Thermal-Mechanical Strain Cycle, 600°F (316°C)⇌1200°F (649°C), Applied to 304 Stainless (Specimen A25A).

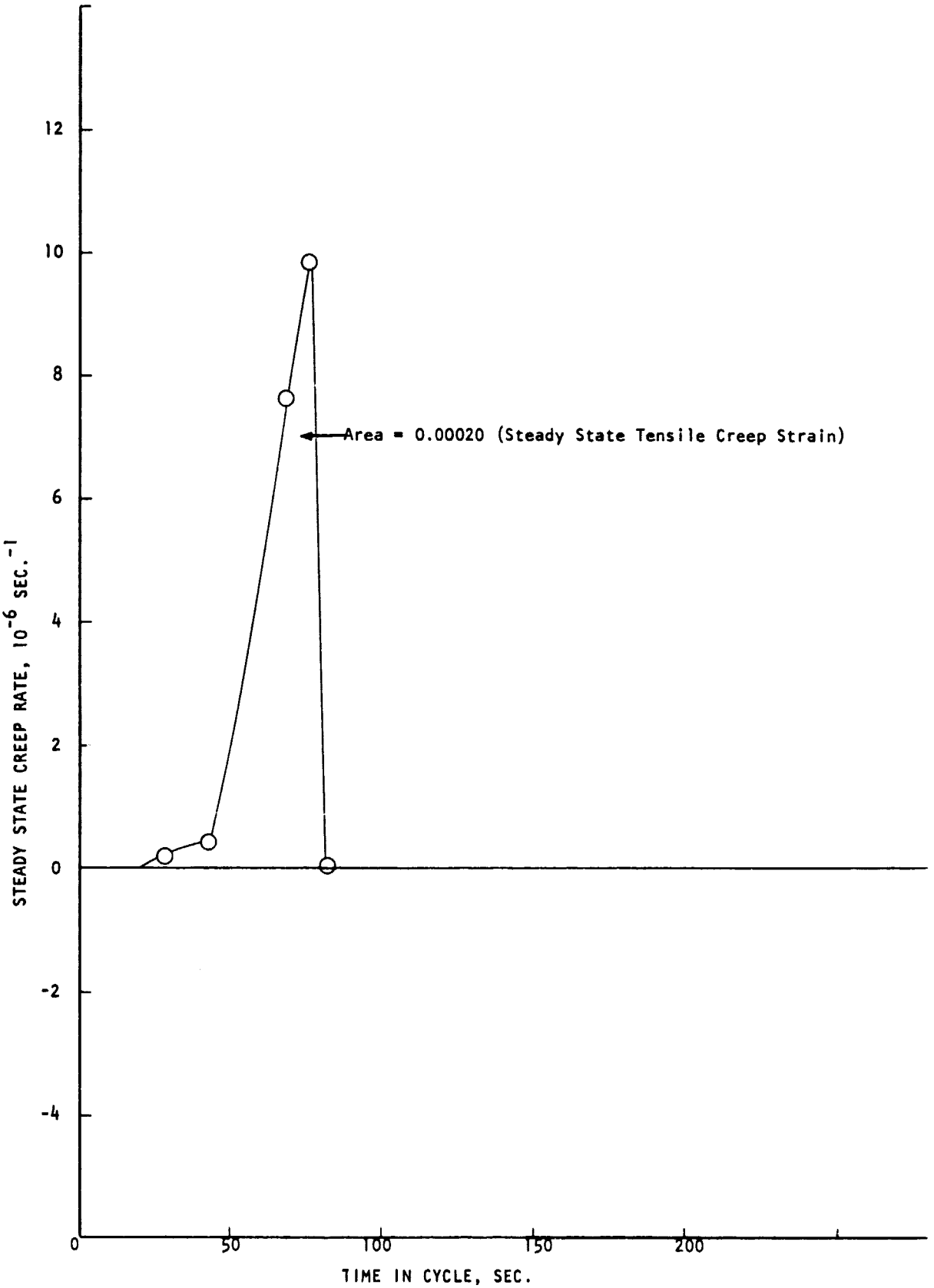

Figure 10. Accumulation of Tensile Steady State Creep Strain During In-Phase, Square-Wave, Thermal-Mechanical, Strain Cycle, 1200°F (649°C)⇄600°F (316°C), Applied to 304 Stainless (Specimen A22A).

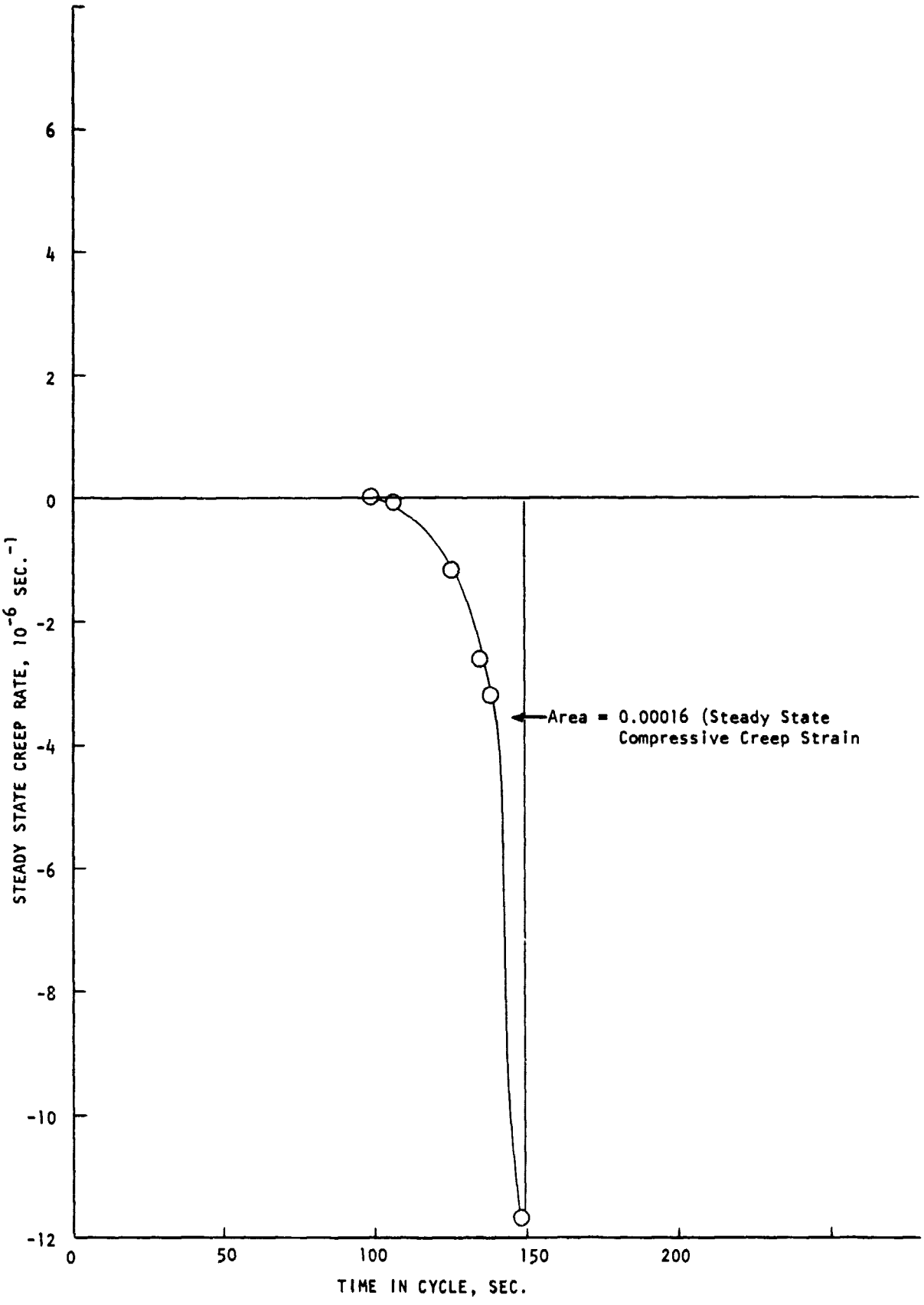

Figure 11. Accumulation of Compressive Steady State Creep Strain During Out-of-Phase, Square Wave, Thermal-Mechanical, Strain Cycle, 600°F (316°C)$\rightleftharpoons$1200°F (649°C), Applied to 304 Stainless (Specimen A23A).

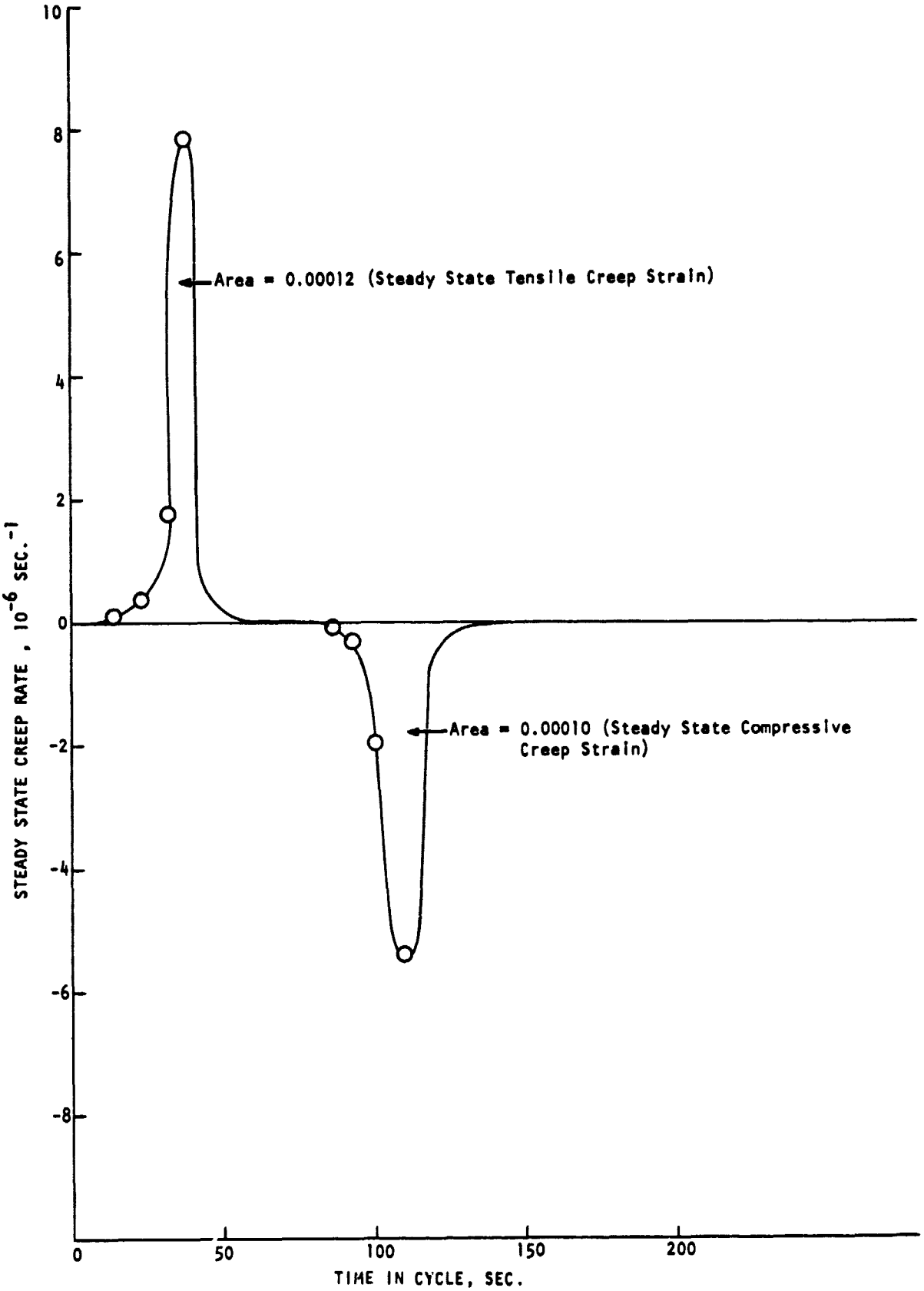

Figure 12. Accumulation of Tensile and Compressive Steady State Creep Strain During Isothermal-Mechanical Strain Cycle, 1100°F (593°C), Applied to A-286 (Specimen L57).

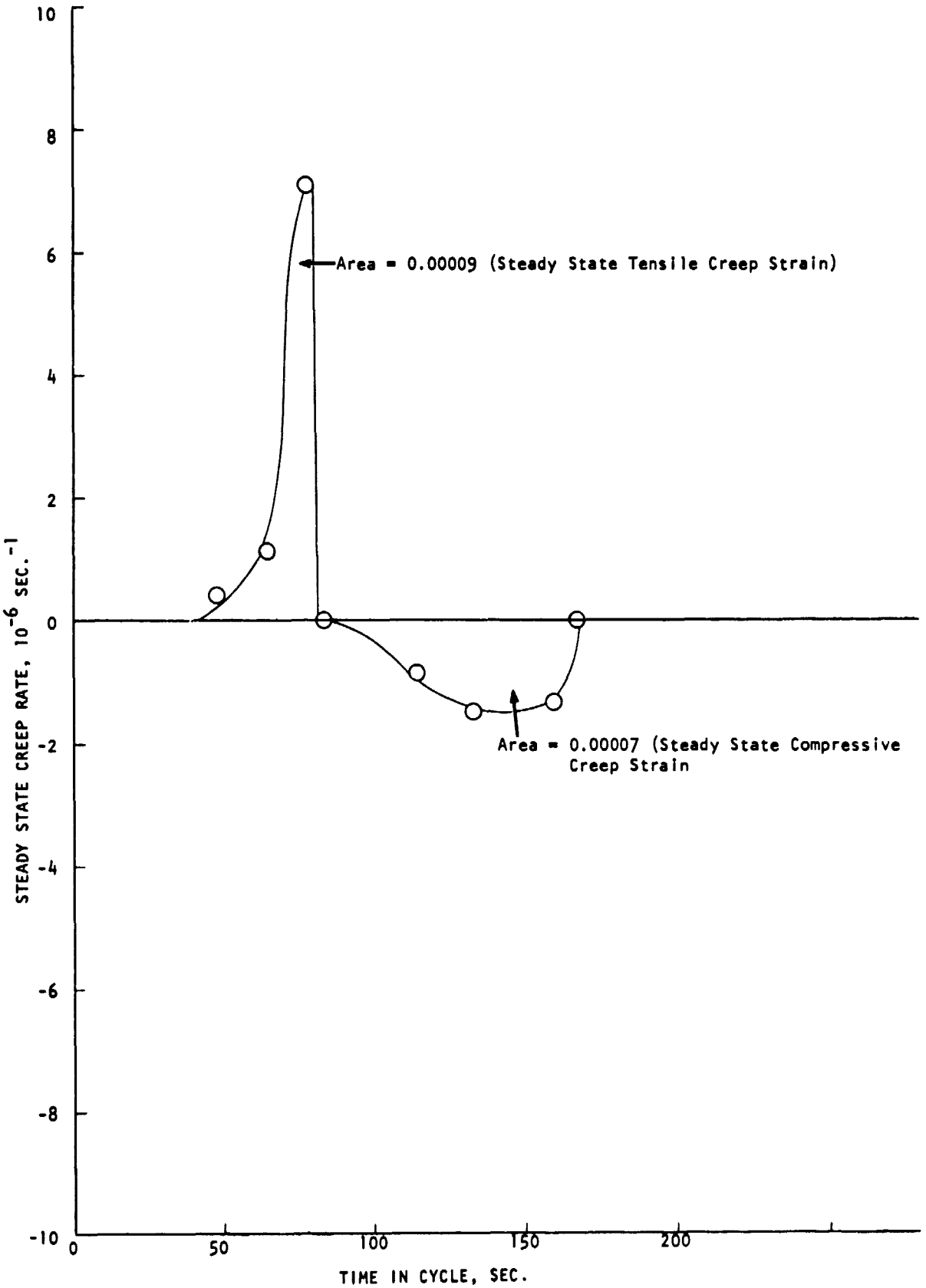

Figure 13. Accumulation of Tensile and Compressive Steady State Creep Strain During In-Phase, Thermal-Mechanical Strain Cycle, 1100°F (593°C) ⇌ 600°F (316°C), Applied to A-286 (Specimen L61).

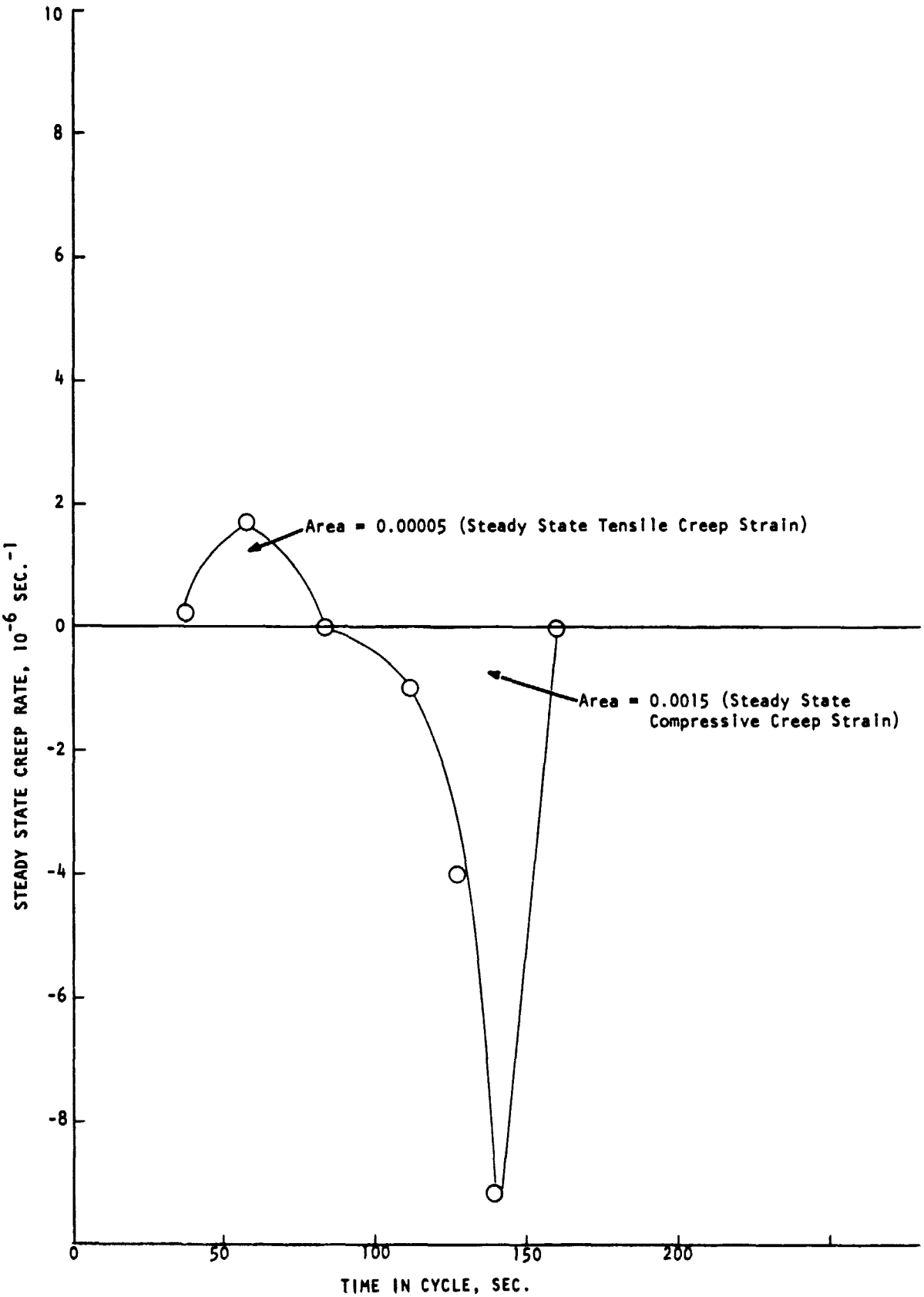

Figure 14. Accumulation of Tensile and Compressive Steady State Creep During Out-of-Phase, Thermal-Mechanical, Strain Cycle, 600°F (316°C)$\rightleftharpoons$ 1100°F (593°C), Applied to A-286 (Specimen L62).

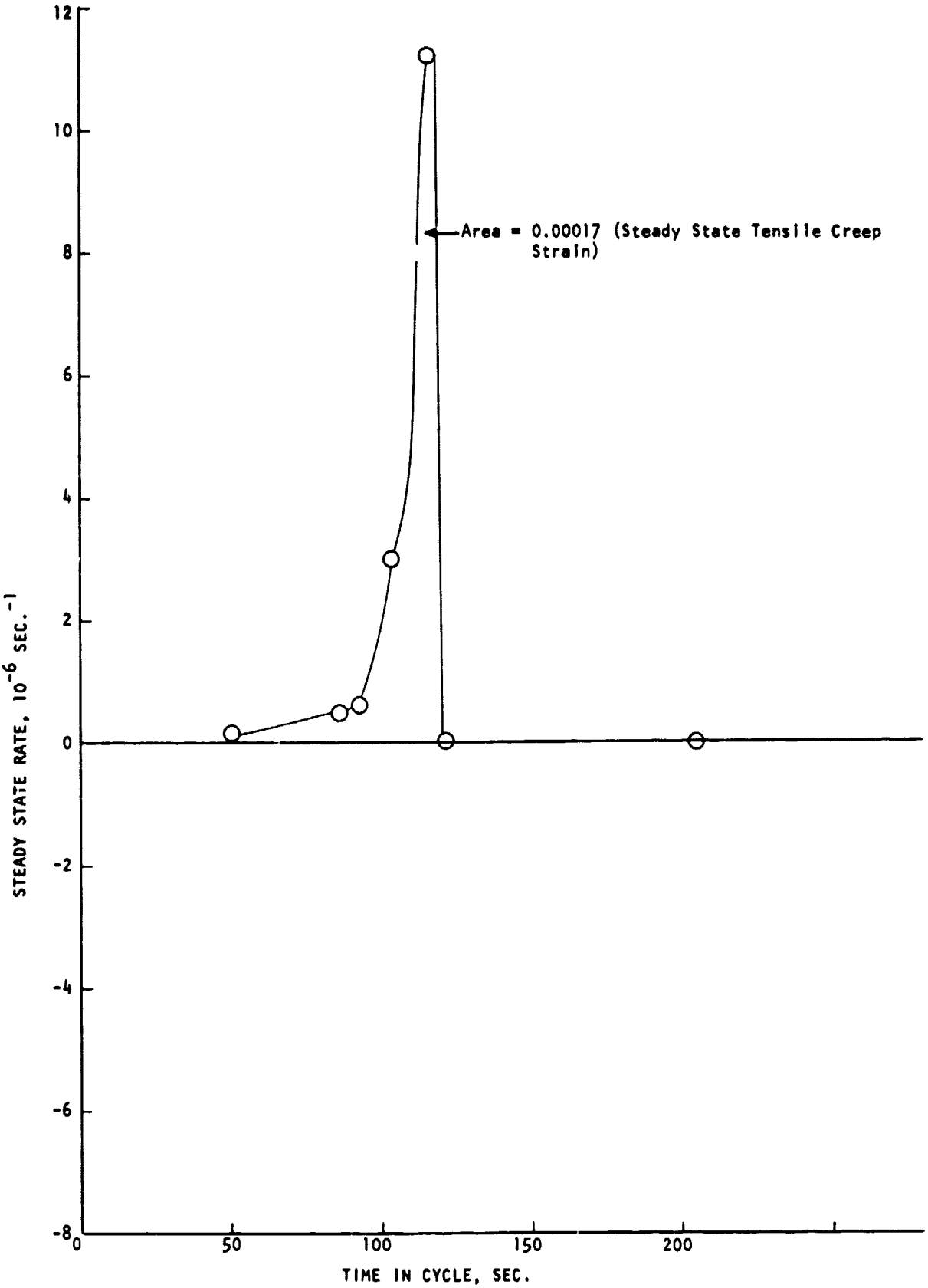

Figure 15. Accumulation of Tensile Steady State Creep Strain During In-Phase Square-Wave, Thermal-Mechanical, Strain Cycle, 1100°F (593°C)⇌ 600°F (316°C), Applied to A-286 (Specimen L58).

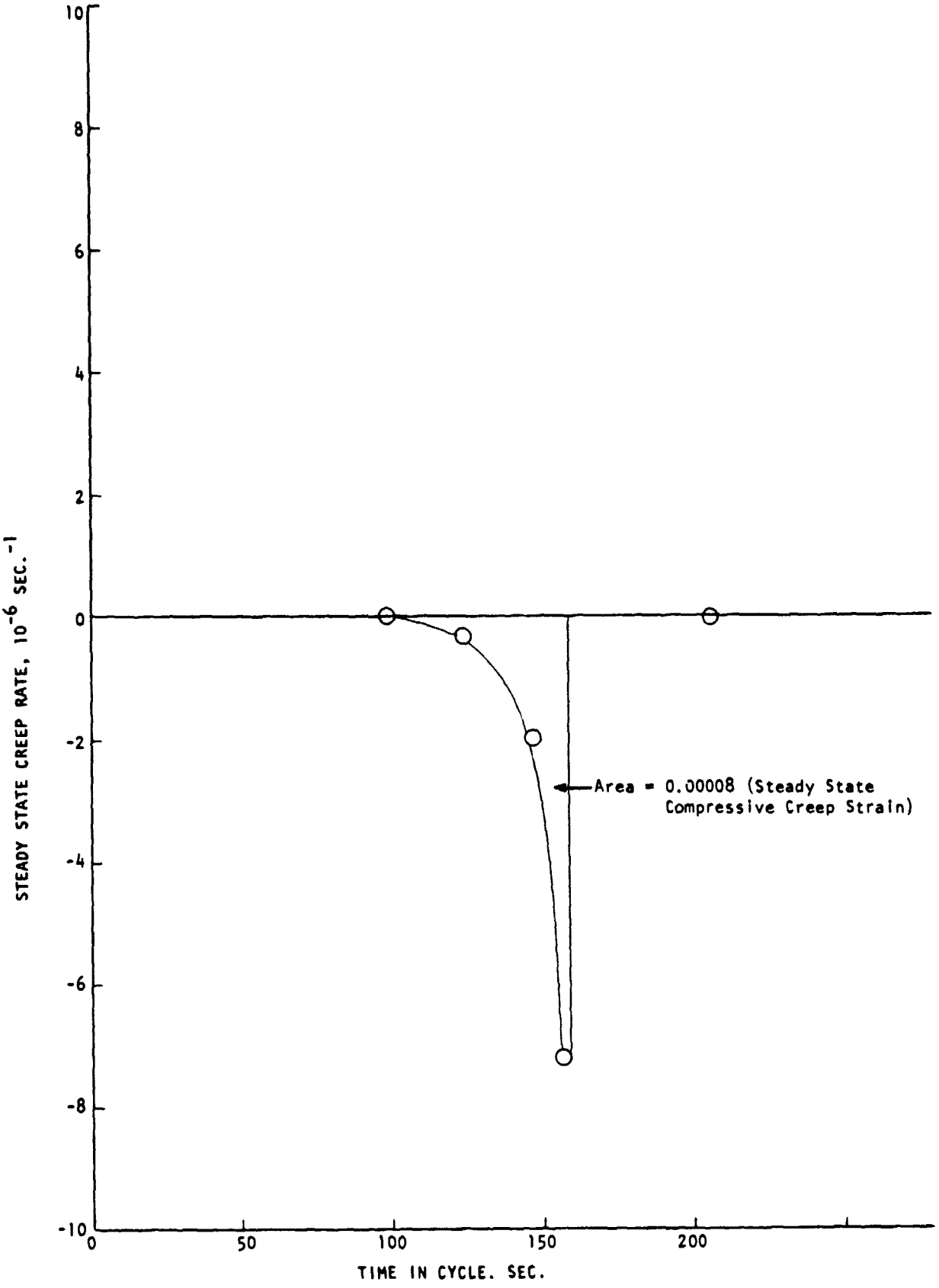

Figure 16. Accumulation of Compressive Steady State Creep Strain During Out-of-Phase, Square-Wave, Thermal-Mechanical, Strain Cycle, 600°F (316°C)$\rightleftharpoons$1100°F (593°C), Applied to A-286 (Specimen L59).

where $\Delta\varepsilon_{in} = \Delta\varepsilon_{pp} + \Delta\varepsilon_{cc} + \Delta\varepsilon_{cp} = 0.02560$

The strainrange fractions are:

$$F_{pp} = \Delta\varepsilon_{pp}/\Delta\varepsilon_{in} = \frac{0.02542}{0.02560} = 0.993$$

$$F_{cc} = \Delta\varepsilon_{pp}/\Delta\varepsilon_{in} = \frac{0.00005}{0.02560} = 0.002$$

$$F_{cp} = \Delta\varepsilon_{cp}/\Delta\varepsilon_{in} = \frac{0.00013}{0.02560} = 0.005$$

B. Analytical Procedure for the Development of the Basic Strainrange Partitioning Life Relationships

From the strainrange partitioning data presented in Table II and utilizing the procedure described in the above example the strainrange fractions can be calculated for each of the fatigue tests conducted in this study. The strain fractions are used in the interaction damage rule which can be written as:

$$\frac{F_{pp}}{N_{pp}} + \frac{F_{cc}}{N_{cc}} + \frac{F_{cc}}{N_{cp}} + \frac{F_{pc}}{N_{pc}} = \frac{1}{N_{pr}}$$

where N_{pp}, N_{cc}, N_{cp}, N_{pc} are the cyclic lives determined from entering the life relationships at a strainrange equal to the entire inelastic strainrange of the cycle of interest, and N_{pr} is the predicted life. A schematic illustration of typical partioned strainrange-life relationships used to characterize material in the creep-fatigue range are shown in Figure 17 (8). These curves are based upon the use of the interaction damage rule and the interpretation of creep strain as being only the steady- state (secondary) portion of the time-dependent strain. Once the life relationships for a specific material are known, the predicted fatigue life for a complicated thermal mechanical strain cycle can be determined by partitioning the hysteresis loop into its inelastic components and applying the interaction damage rule.

In the work done previously at TRW on ASTAR 811C, 304 stainless and A-286 (6,7), however, the basic life relationships were not determined prior to conducting complex thermal mechanical strain cycling tests. An example of the typical results obtained in these programs is shown in Figure 18, which includes the fatigue life results for A-286 alloy. Similar results are also available for ASTAR 811C and 304 stainless. The results of these programs can be utilized along with the strainrange data developed in the present study to develop the basic life relationships by analytical methods. For example, assume that the basic life relationships for A-286 can be represented in reality by the series of lines shown in Figure 17. At this point, however, only the pp line is known

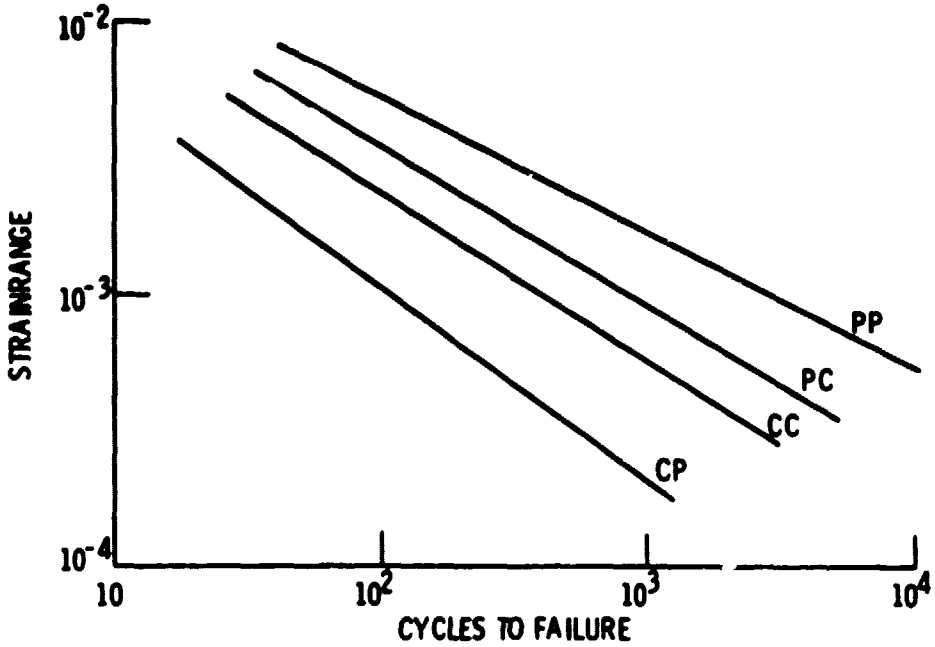

Figure 17. Typical Partitioned Strainrange-Life Relationships Used to Characterize Material Behavior in the Creep-Fatigue Range (8).

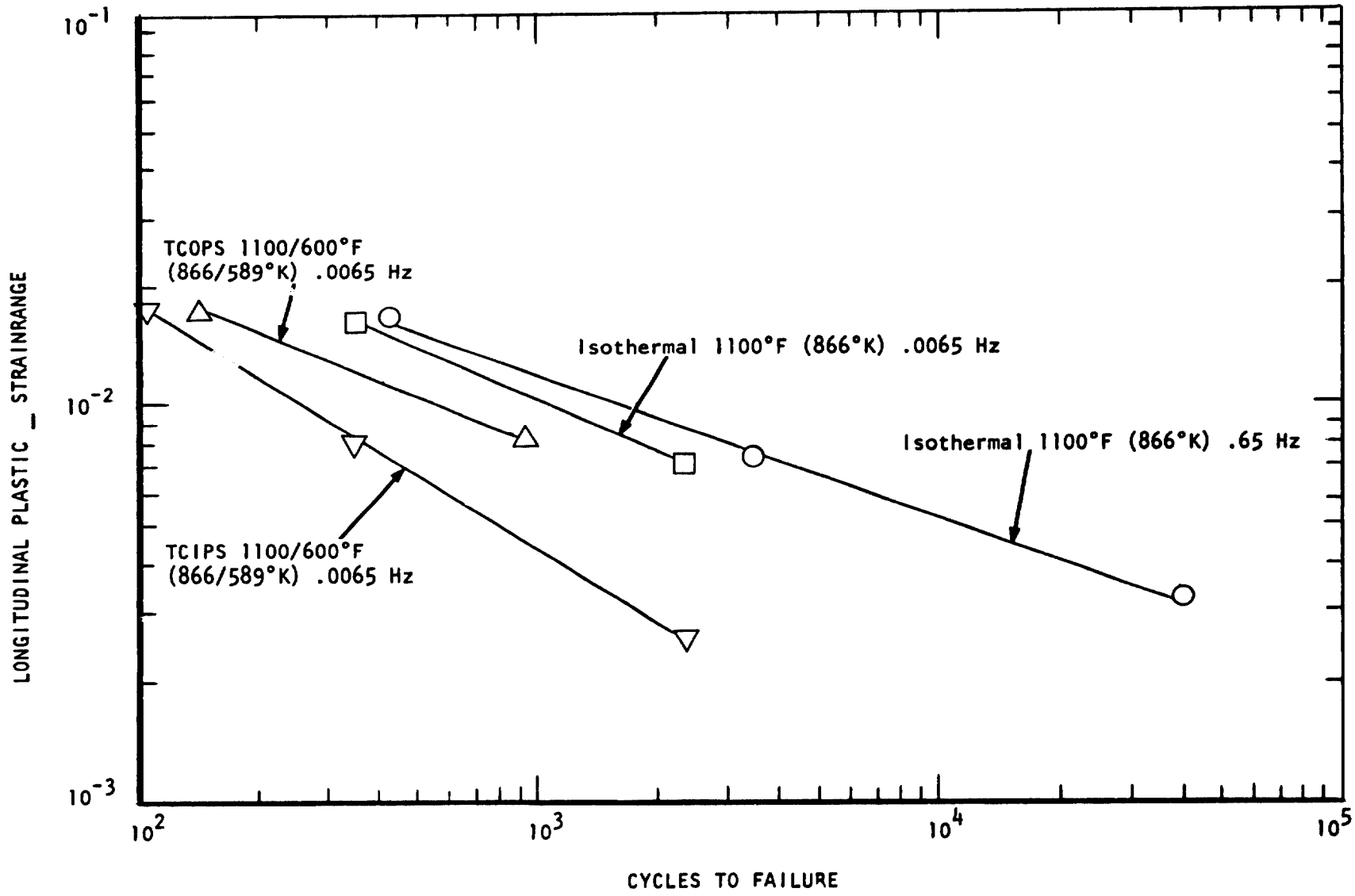

Figure 18. A-286 Fatigue Life Results (7).

with any degree of certainty. This pp line can be taken to be the isothermal data presented in Figure 18 for tests conducted at 1100°F (593°C) and 0.65 Hz. It is generally accepted that in tests conducted at this frequency essentially all of the damage is of the pp type. In the isothermal test duplicated in the present program at 0.0065 Hz, however, damage consists of both the pp and the cc type. The interaction damage rule for this complicated test can be written as:

$$\frac{1}{N_f} = \frac{F_{pp}}{N_{pp}} + \frac{F_{cc}}{N_{cc}}$$

where N_f is the failure time from the 0.0065 Hz isothermal line from Figure 18 for the particular inelastic strainrange, F_{pp} and F_{cc} are the partitioned inelastic strainranges given in Table II and N_{pp} is the failure time from the 0.65 Hz isothermal line from Figure 18 for the particular inelastic strainrange. This equation can now be solved for N_{cc}. In this example (Specimen L57), the inelastic strainrange is 0.01740, $F_{pp} = 0.99$, $F_{cc} = 0.01$, and $N_{pp} = 350$. Solving the equation for N_{cc} indicates a value of 20 cycles to failure. This data point thus represents the first point on the assumed cc line for A-286 shown in Figure 17.

To extend this analytical method further, consider the TCIP test conducted for A-286 at 0.0065 Hz reported in Table II. In this particular test, pp, cc and cp damage were all obtained. The interaction damage rule for this thermal mechanical test can be written as:

$$\frac{1}{N_f} = \frac{F_{pp}}{N_{pp}} + \frac{F_{cc}}{N_{cc}} + \frac{F_{cp}}{N_{cp}}$$

All of the strainrange fractions are known. N_f and N_{pp} can be obtained from the data presented in Figure 18 for A-286. Although only one data point exists for the N_{cc} line, a first assumption can be made as to the slope of this line and N_{cc} can then be estimated at the particular inelastic strainrange. The equation can now be solved for N_{cp} resulting in a first approximation for this value. In a similar manner, the partitioned TCOP test results can be used to develop a first approximation for the N_{pc} line. Utilizing the partitioned strainrange data for each of the tests conducted on A-286, ASTAR 811C and 304 stainless during the present study, an iterative or step-wise analytical development of the basic life relationships can be established for these alloys.

C. Creep Stress Versus Steady State Creep Rate Plots

Plots of creep stress versus steady state creep rate for each specimen are shown in Figures 19-21. Each figure contains data for a particular alloy and includes the steady state creep rates measured at the various temperatures.

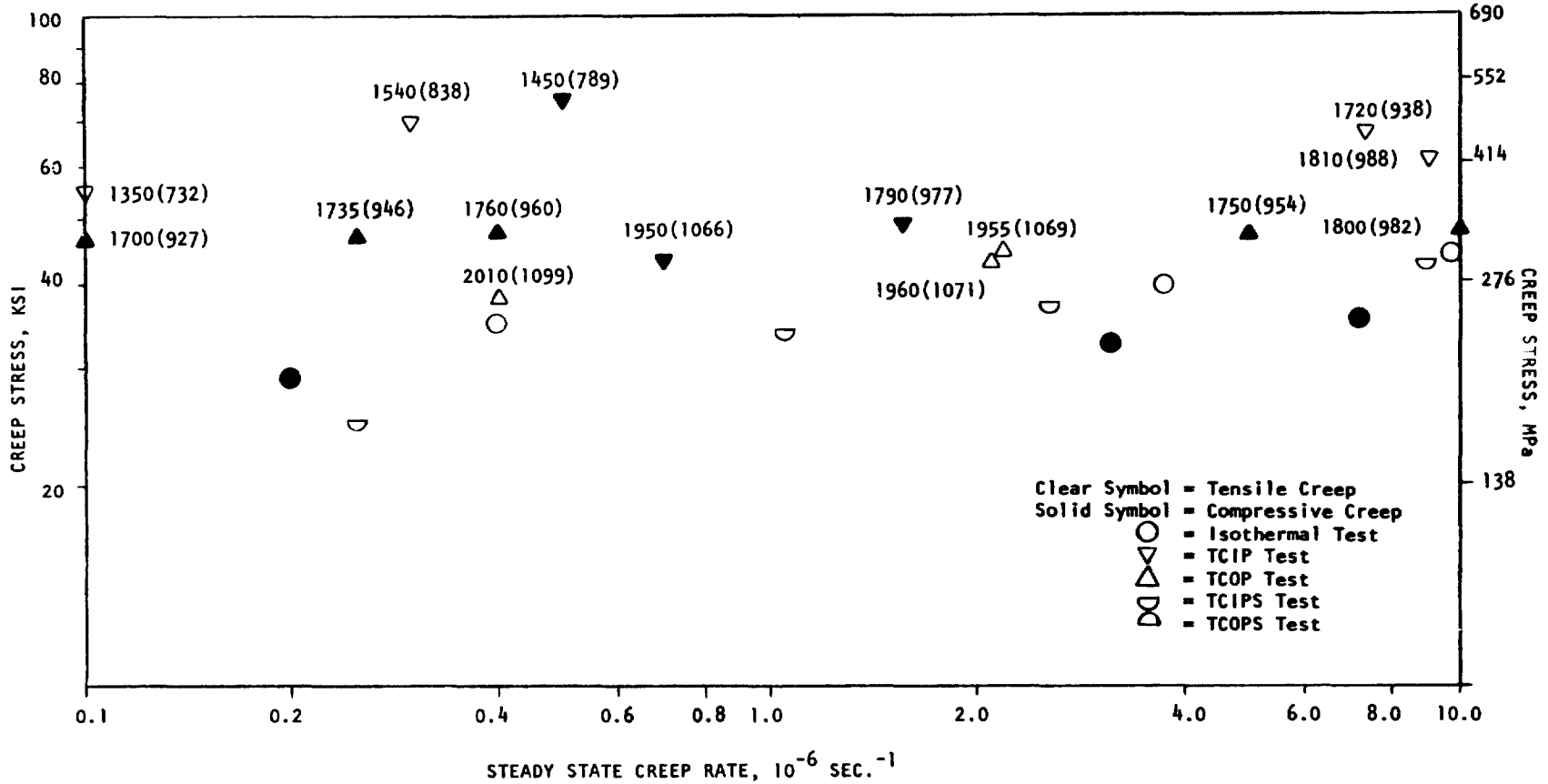

Figure 19. Plot of Steady State Creep Rate Versus Creep Stress for all the Conditions of Stress and Temperature Encountered in the Program for ASTAR 811C. Isothermal Tests Were Conducted at 2100°F (1149°C). In Instances Where Creep Stresses Were Applied at Other Temperatures, These Have Been Indicated in °F (°C) on the Graph.

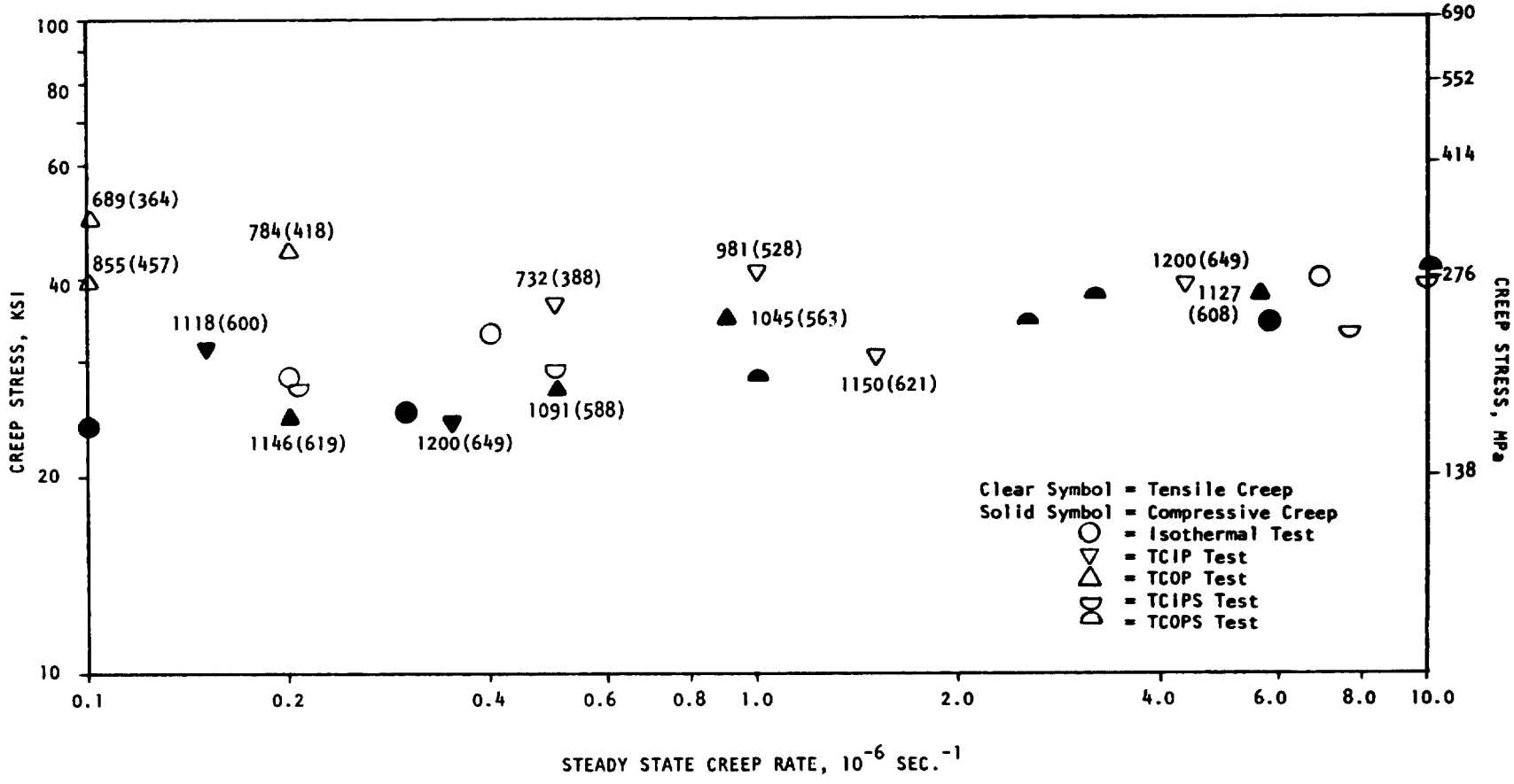

Figure 20. Plot of Steady State Creep Rate Versus Creep Stress for all the Conditions of Stress and Temperature Encountered in the Program for 304 Stainless. Isothermal Tests Were Conducted at 1200°F (649°C). In Instances Where Creep Stresses Were Applied at Other Temperatures, These Have Been Indicated in °F (°C) on the Graph.

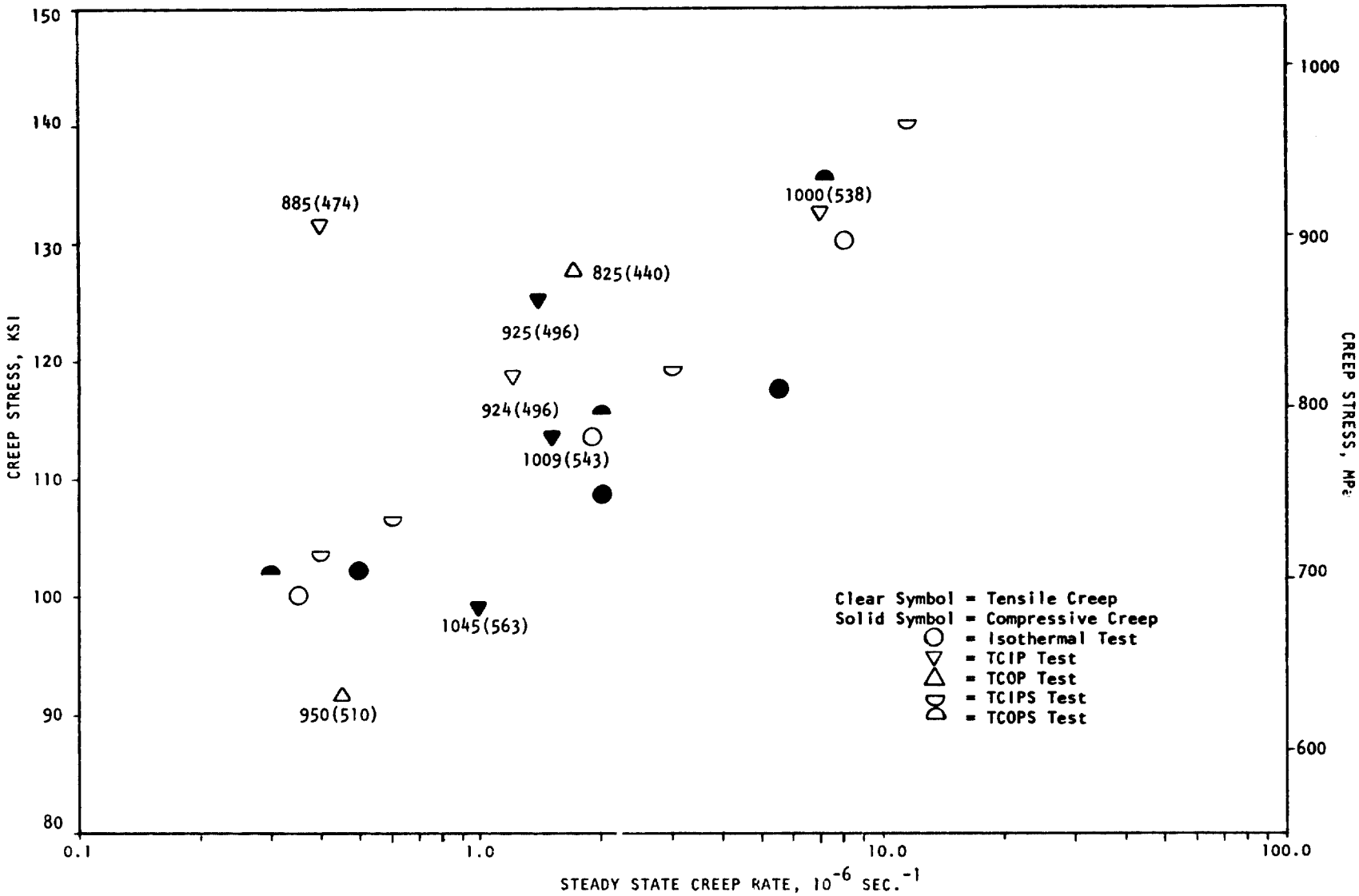

Figure 21. Plot of Steady State Creep Rate Versus Creep Stress for all the Conditions of Stress and Temperature Encountered in the Program for A-286. Isothermal Tests Were Conducted at 1100°F (593°C). In Instances Where Creep Stresses Were Applied at Other Temperatures, These have Been Indicated in °F (°C) on the Graph.

IV REFERENCES

1. S. S. Manson, G. R. Halford and M. H. Hirschberg, "Creep-Fatigue Analysis by Strainrange Partitioning," Design for Elevated Temperature Environment, ASME, 1971, pp 12-44, DISC, pp. 25-28.

2. G. R. Halford, M. H. Hirschberg and S. S. Manson, "Temperature Effects on the Strainrange Partitioning Approach for Creep-Fatigue Analysis," Fatigue at Elevated Temperatures, ASTM STP 520, American Society for Testing and Materials, 1973, pp. 658-667, DISC, pp. 668-669.

3. S. S. Manson. "The Challange to Unify Treatment of High Temperature Fatigue - A Partisan Proposal Based on Strainrange Partitioning," Fatigue at Elevated Temperatures, ASTM STP 520, American Society for Testing and Materials, 1973, pp 744-775, DISC, pp. 775-782.

4. S. S. Manson, G. R. Halford, and A. J. Nactigall, "Separation of the Strain Components for use in Strainrange Partitioning," NASA TM X-71737, June, 1975.

5. G. R. Halford and S. S. Manson, "Life Prediction of Thermal-Mechanical Fatigue Using Strainrange Partitioning," NASA TM X-71829, November, 1975.

6. K. D. Sheffler and G. S. Doble, "Influence of Creep Damage on the Low Cycle Thermal-Mechanical Fatigue Behavior of Two Tantalum Base Alloys," Final Report, Contract NAS-3-13228, NASA CR-121001, TRW ER-7592, 1 May 1972.

7. K. D. Sheffler, "Vacuum Thermal-Mechanical Fatigue Testing of Two Iron Base High Temperature Alloys," Topical Report No. 3, Contract NAS-3-6010, NAS-CR-134524, TRW ER-7696, 31 January 1974.

8. M. H. Hirschberg and G. R. Halford, "Strainrange Partitioning - A Tool for Characterizing High Temperature Low Cycle Fatigue," NASA TMX-71691, Paper presented at Fortieth Meeting of the AGARD Structures and Materials Panel of NATO, Brussels, Belgium April 13-18, 1975.

APPENDIX

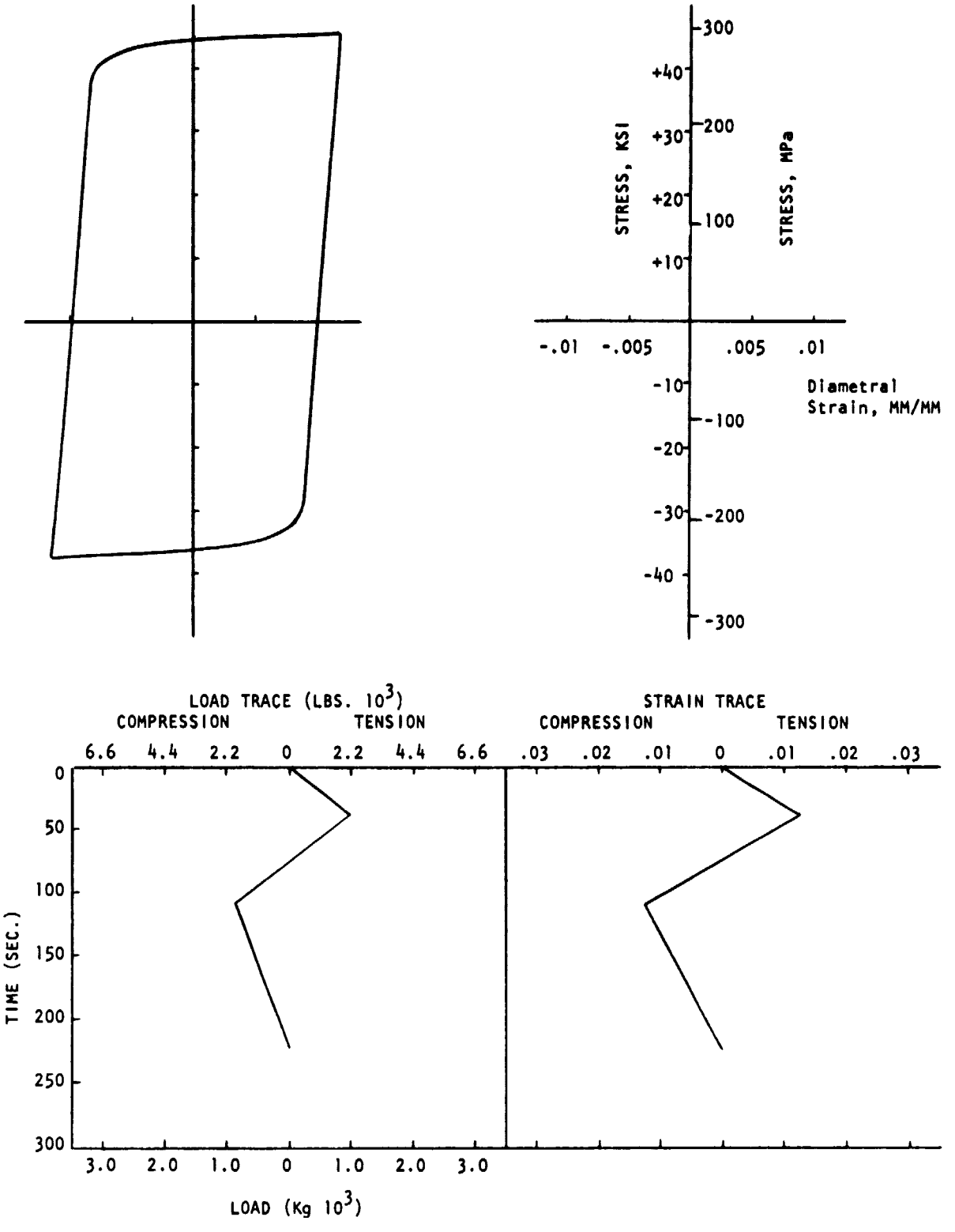

Figure A-1. Hysteresis Loop, Load-Time Trace and Strain Time Trace for ASTAR 811C, Specimen A1D, ISOT Type Test.

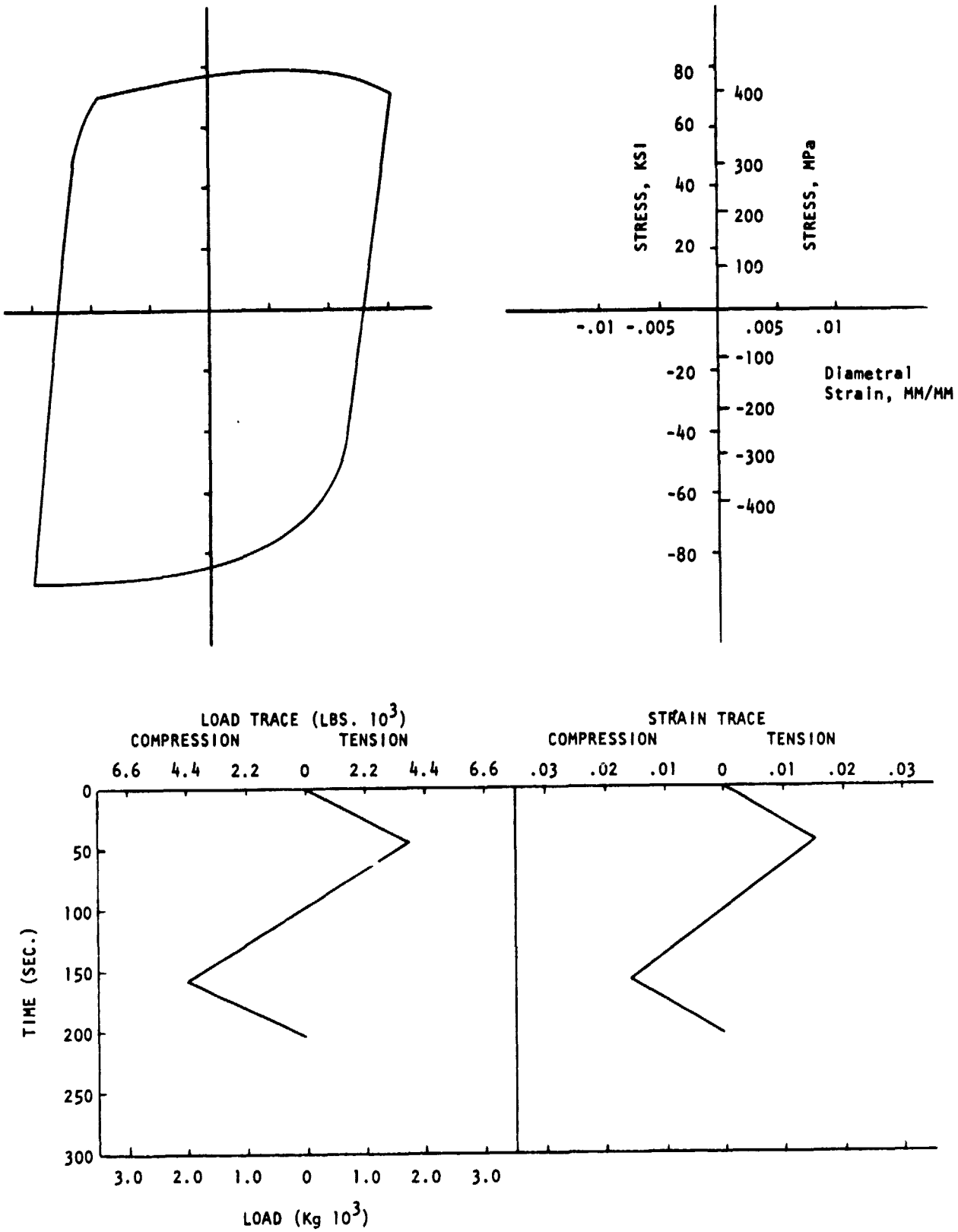

Figure A-2. Hysteresis Loop, Load-Time Trace and Strain Time Trace for ASTAR 811C, Specimen A15D, TCIP Type Test.

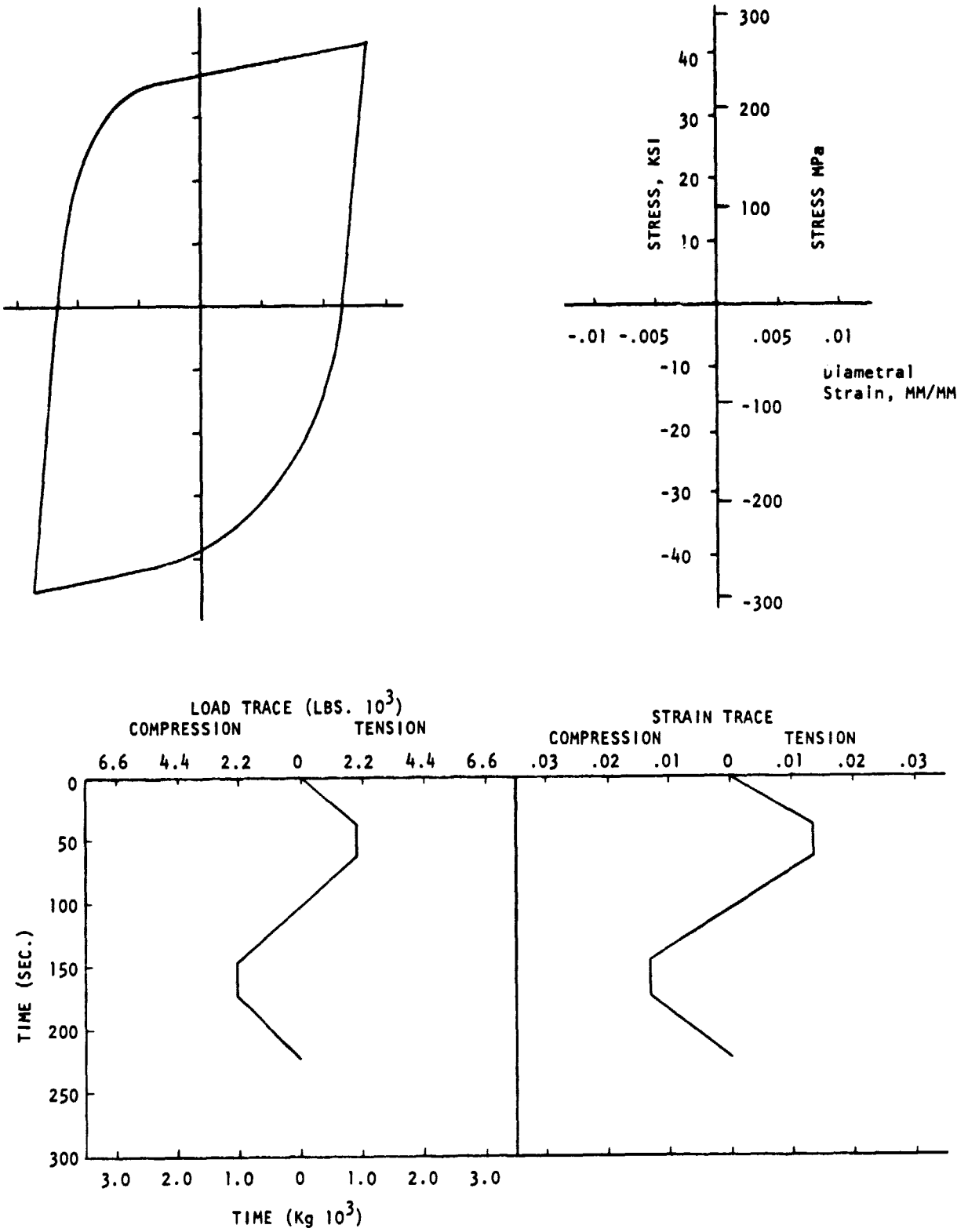

Figure A-3. Hysteresis Loop, Load-Time Trace and Strain Time Trace for ASTAR 811C, Specimen A21D, TCOP Type Test.

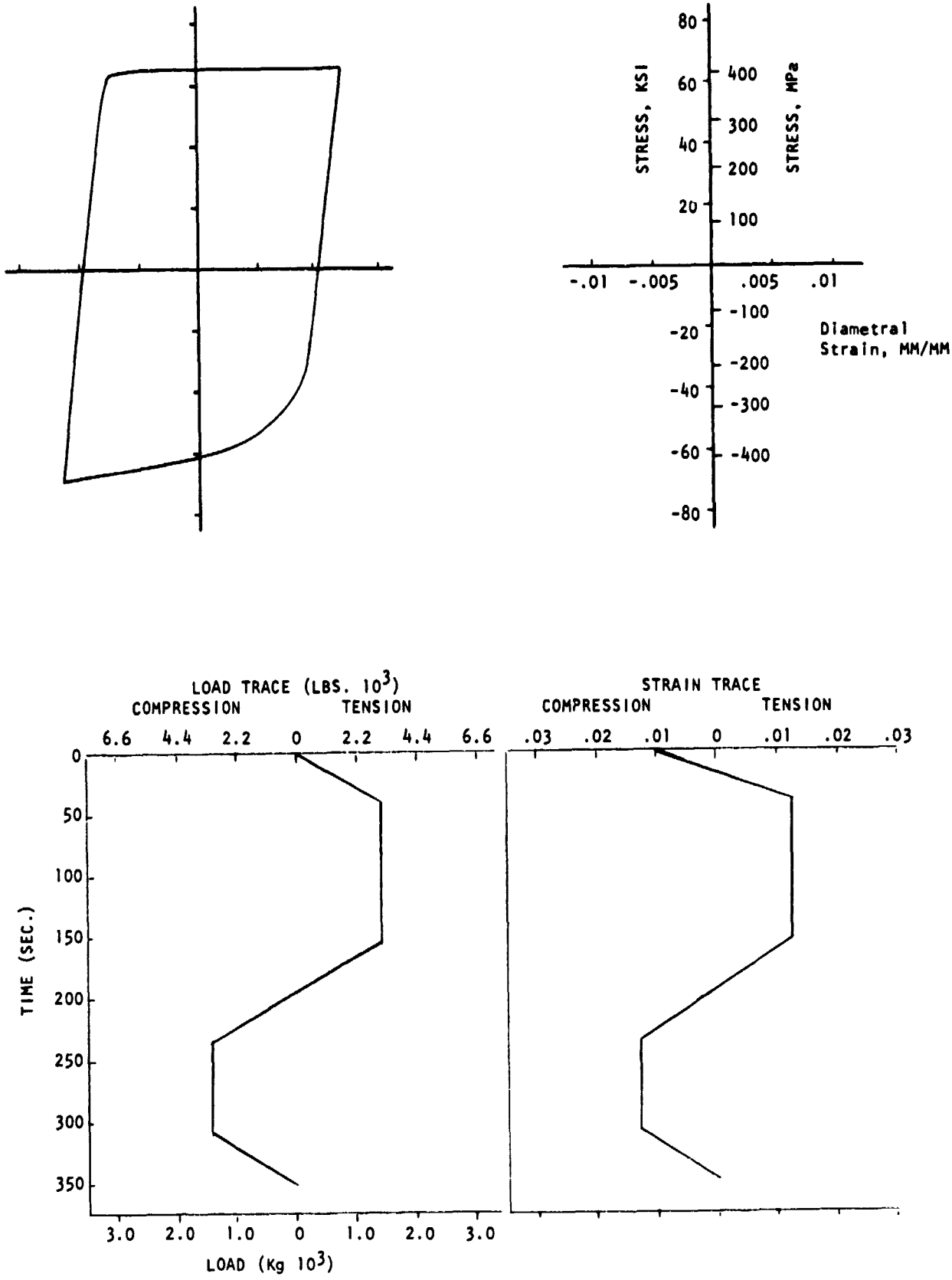

Figure A-4. Hysteresis Loop, Load-Time Trace and Strain Time Trace for ASTAR 811C, Specimen A49D, TCIPS Type Test.

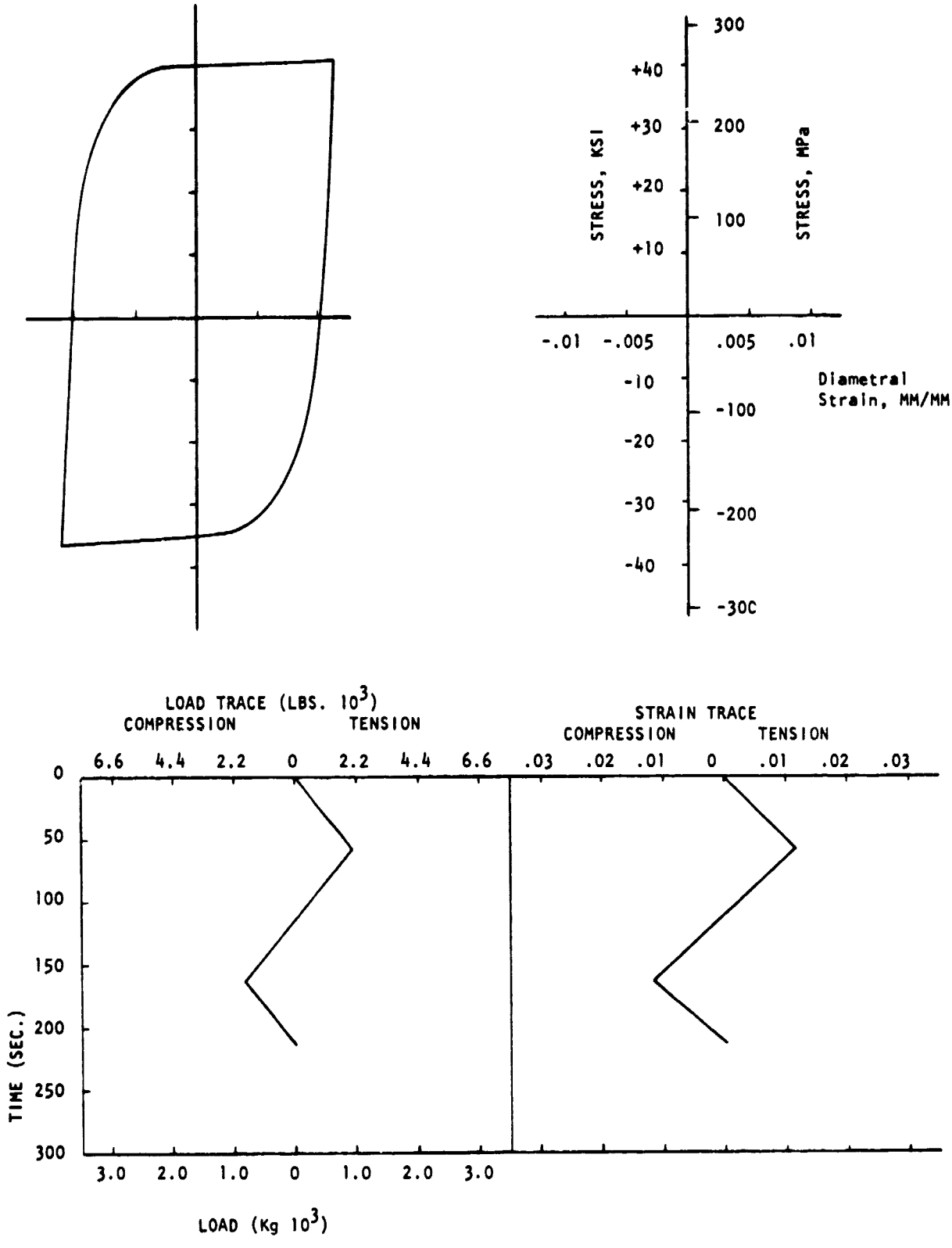

Figure A-5. Hysteresis Loop, Load-Time Trace and Strain Time Trace for 304 Stainless, Specimen A21A, ISOT Type Test.

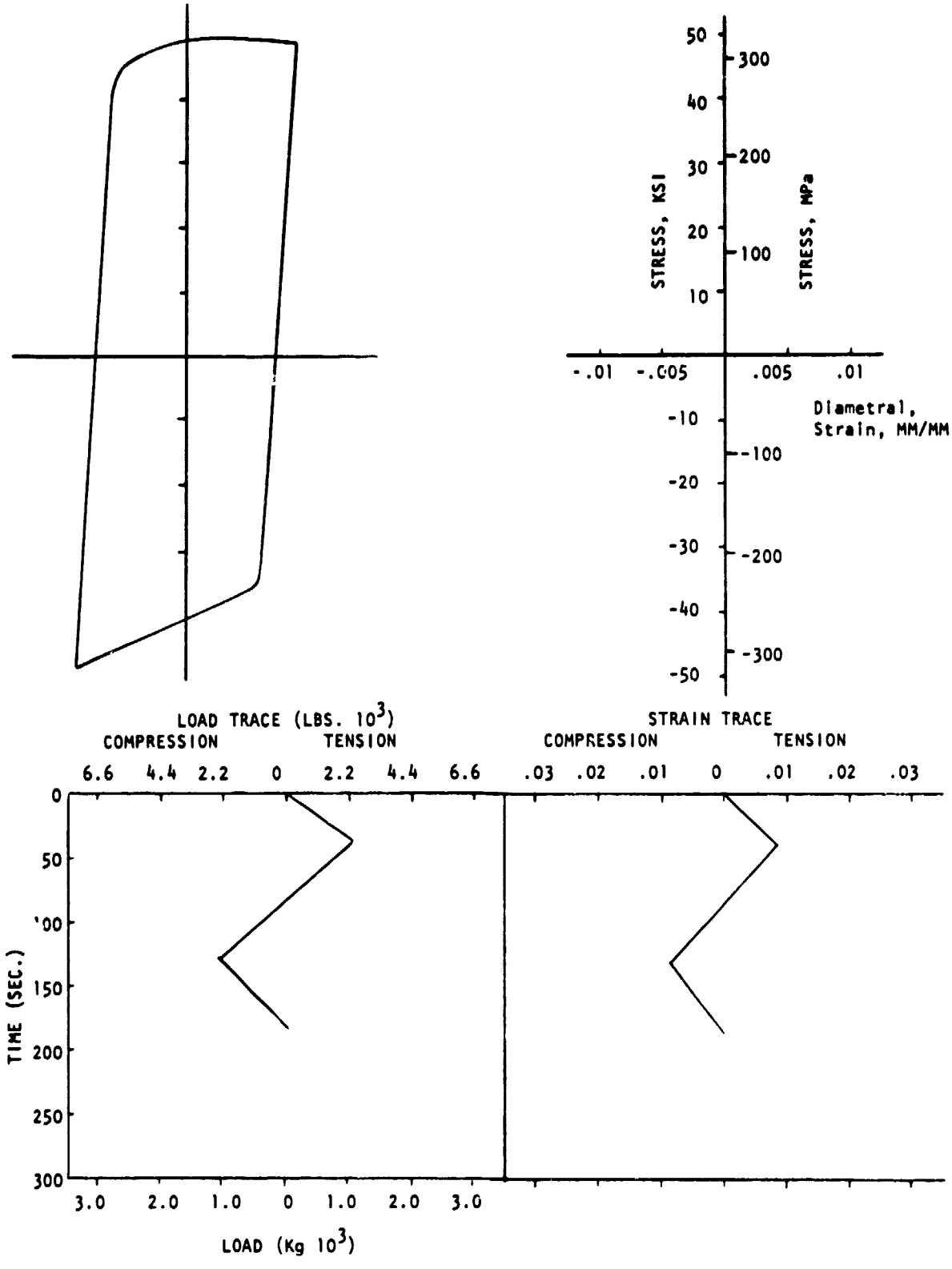

Figure A-6. Hysteresis Loop, Load-Time Trace and Strain Time Trace for 304 Stainless, Specimen A24A, TCIP Type Test.

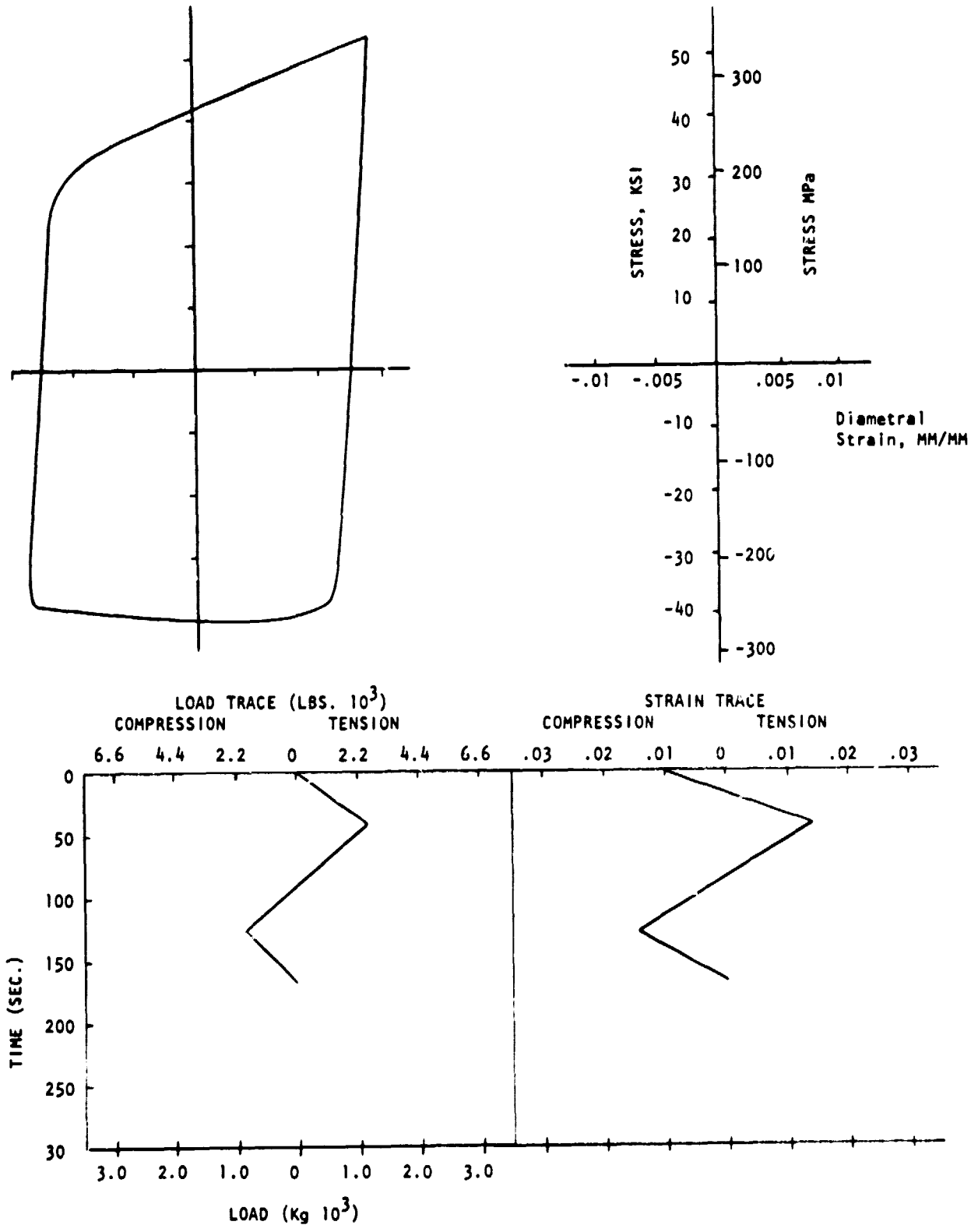

Figure A-7. Hysteresis Loop, Load-Time Trace and Strain Time Trace for 304 Stainless, Specimen A25A, TCOP Type Test.

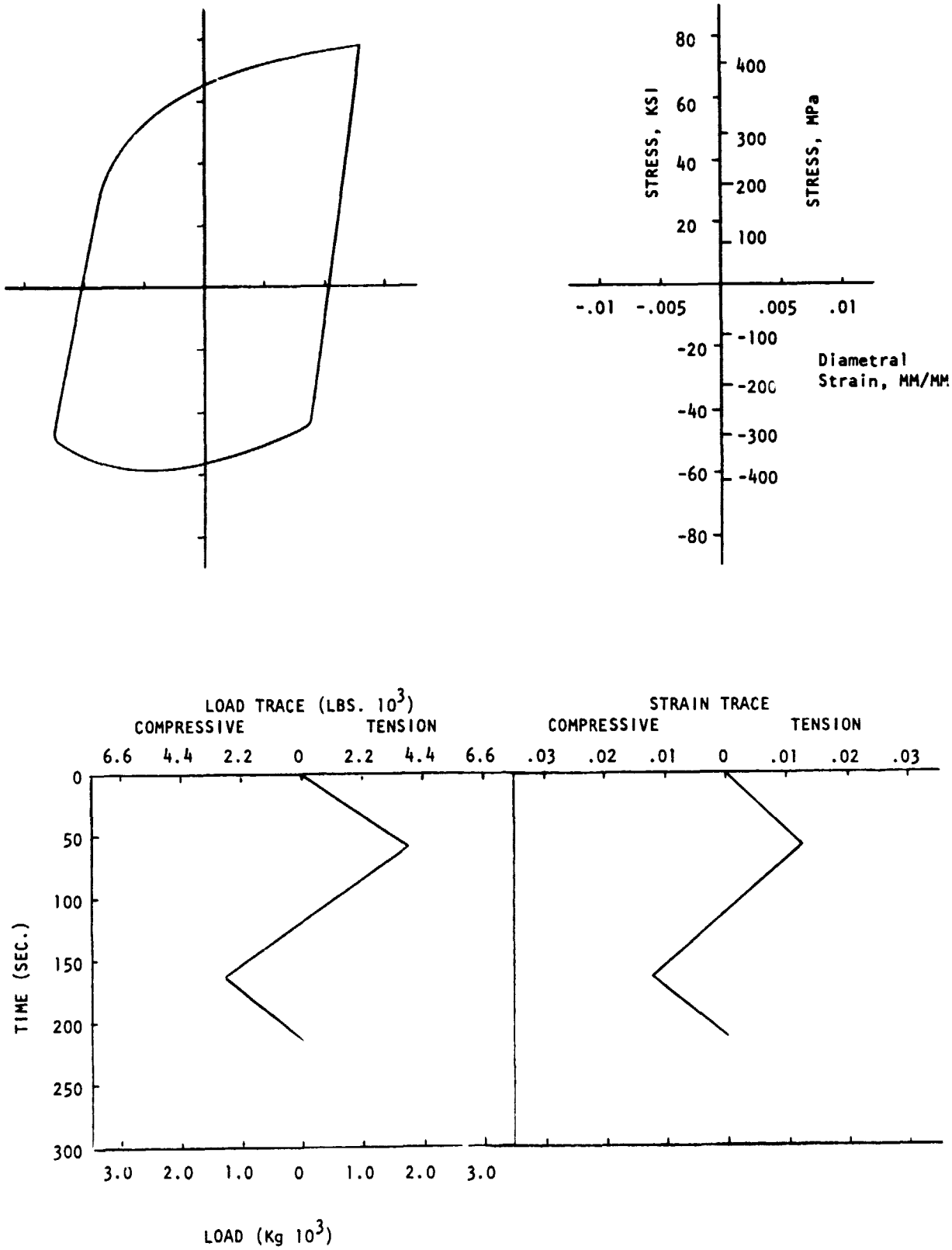

Figure A-8. Hysteresis Loop, Load-Time Trace and Strain Time Trace for 304 Stainless, Specimen A22A, TCIPS Type Test.

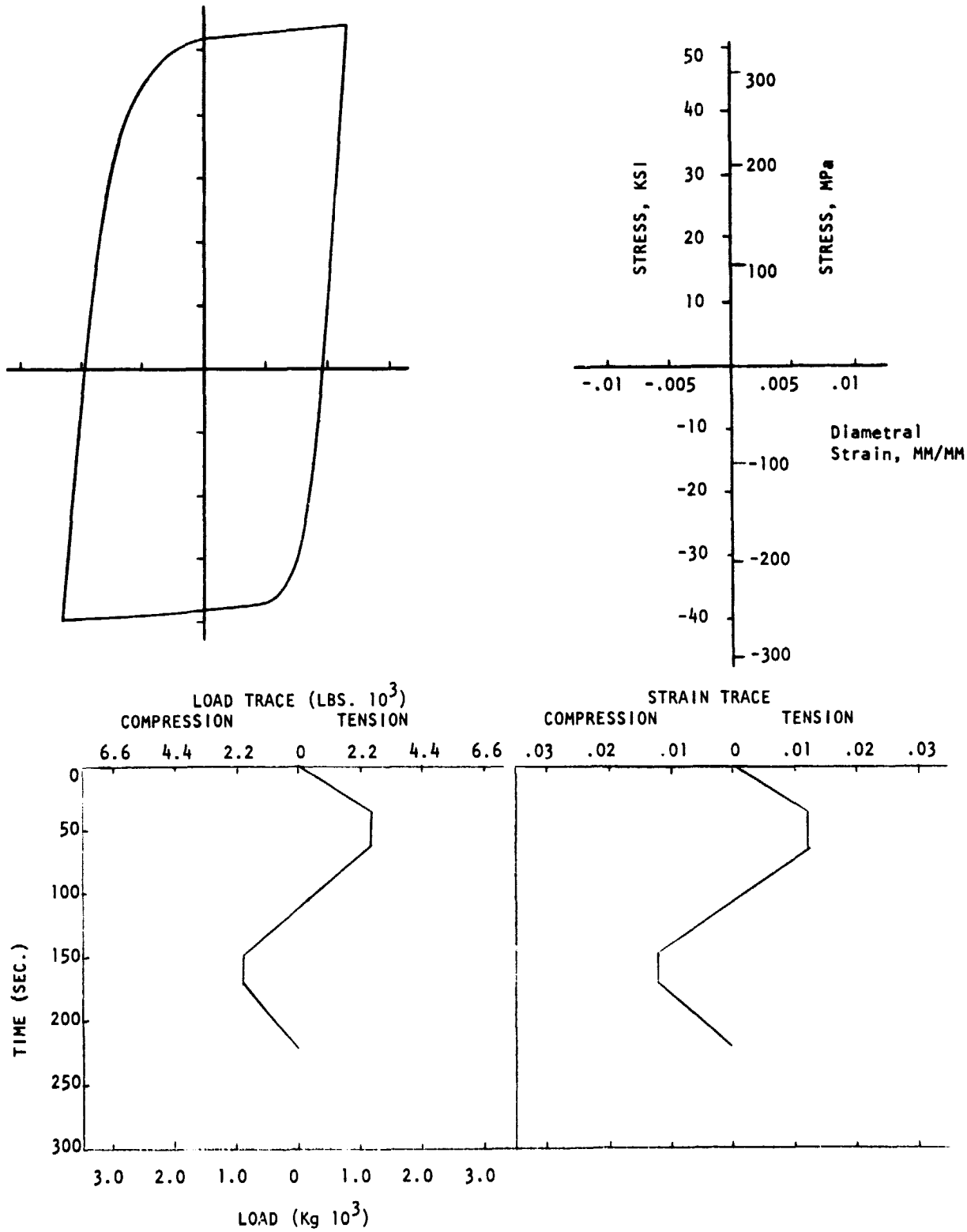

Figure A-9. Hysteresis Loop, Load-Time Trace and Strain Time Trace for 304 Stainless, Specimen A23A, TCOPS Type Test.

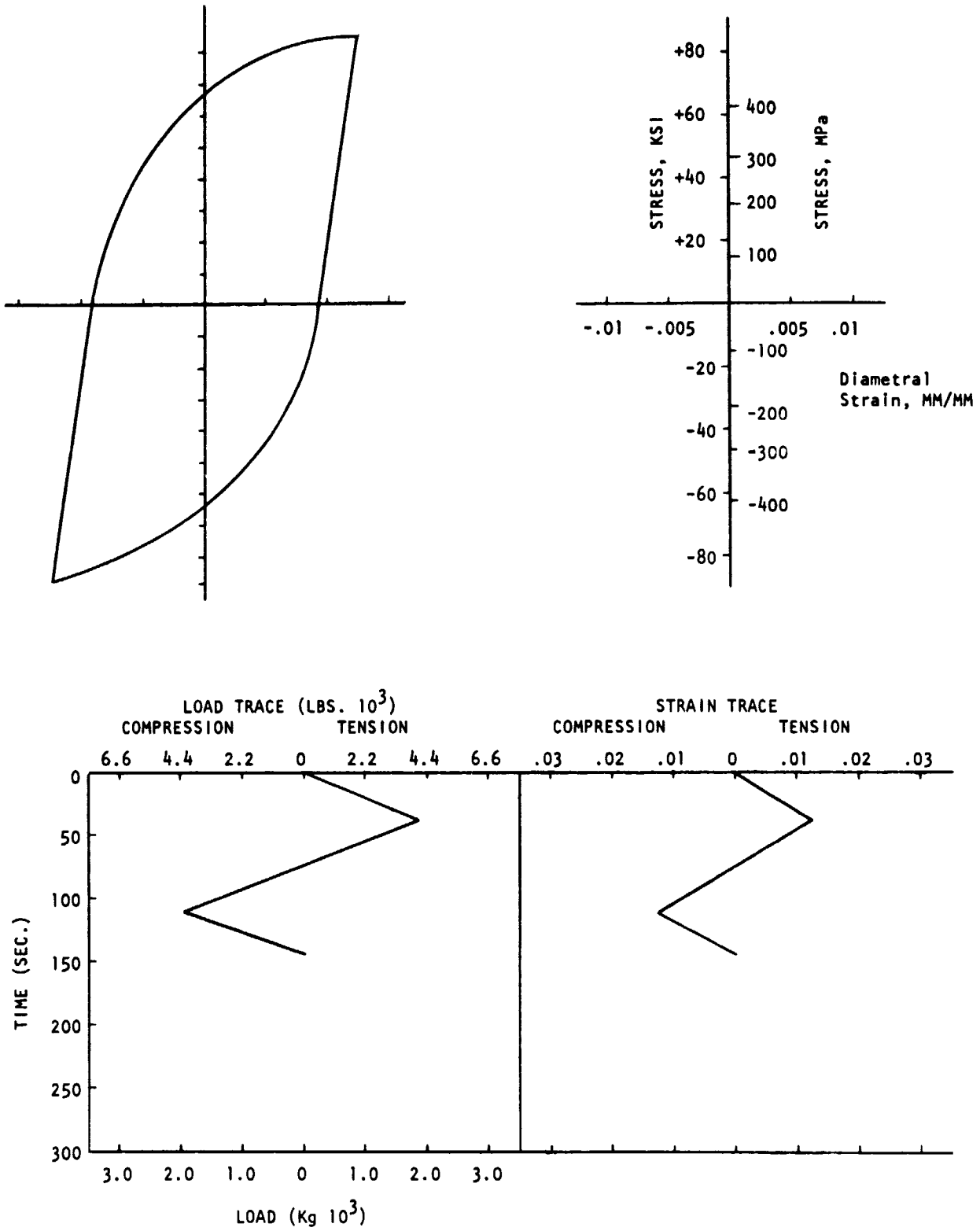

Figure A-10. Hysteresis Loop, Load-Time Trace and Strain Time Trace for A-286, Specimen L57, ISOT Type Test.

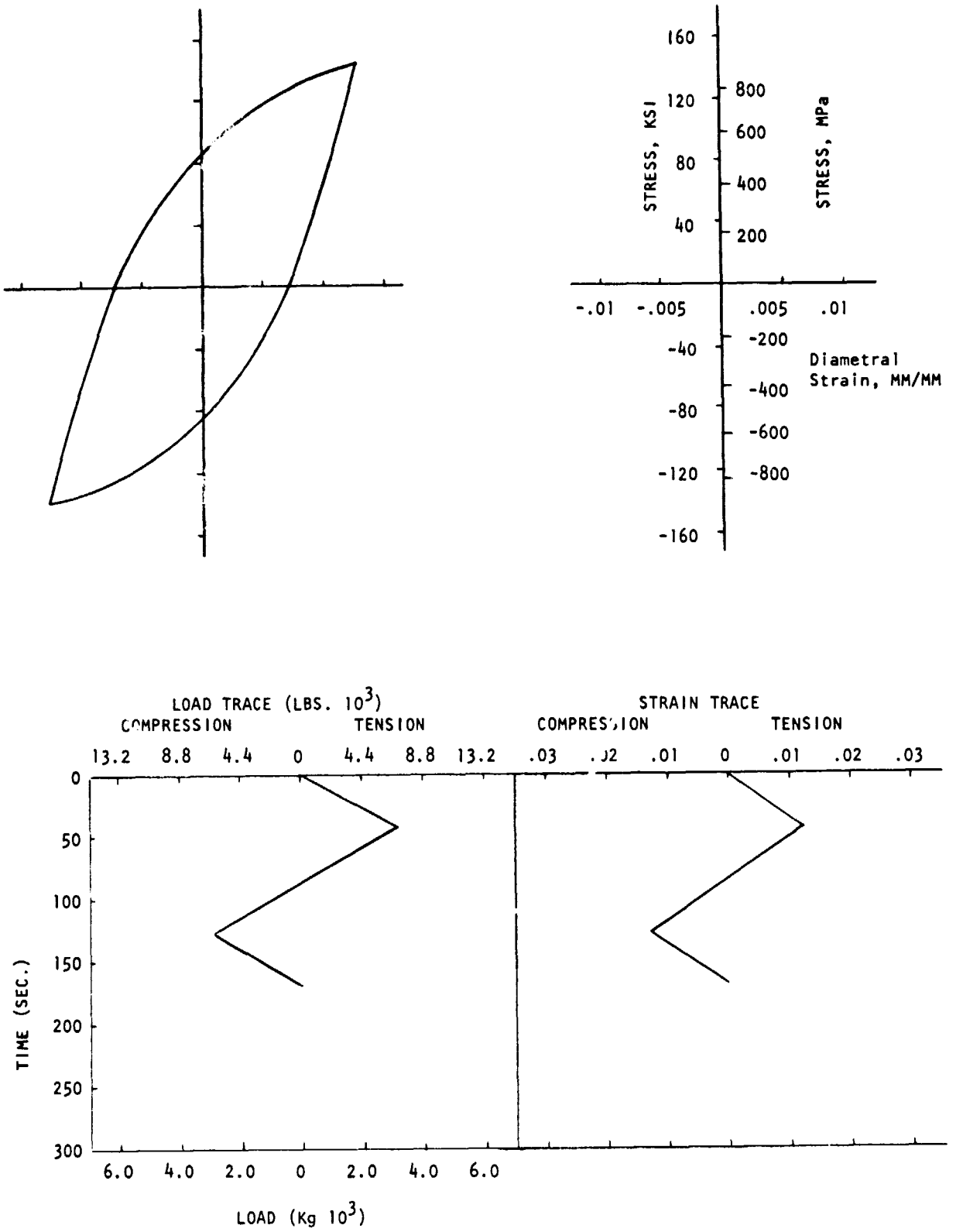

Figure A-11. Hysteresis Loop, Load-Time Trace and Strain Time Trace for A-286, Specimen L61, TCIP Type Test.

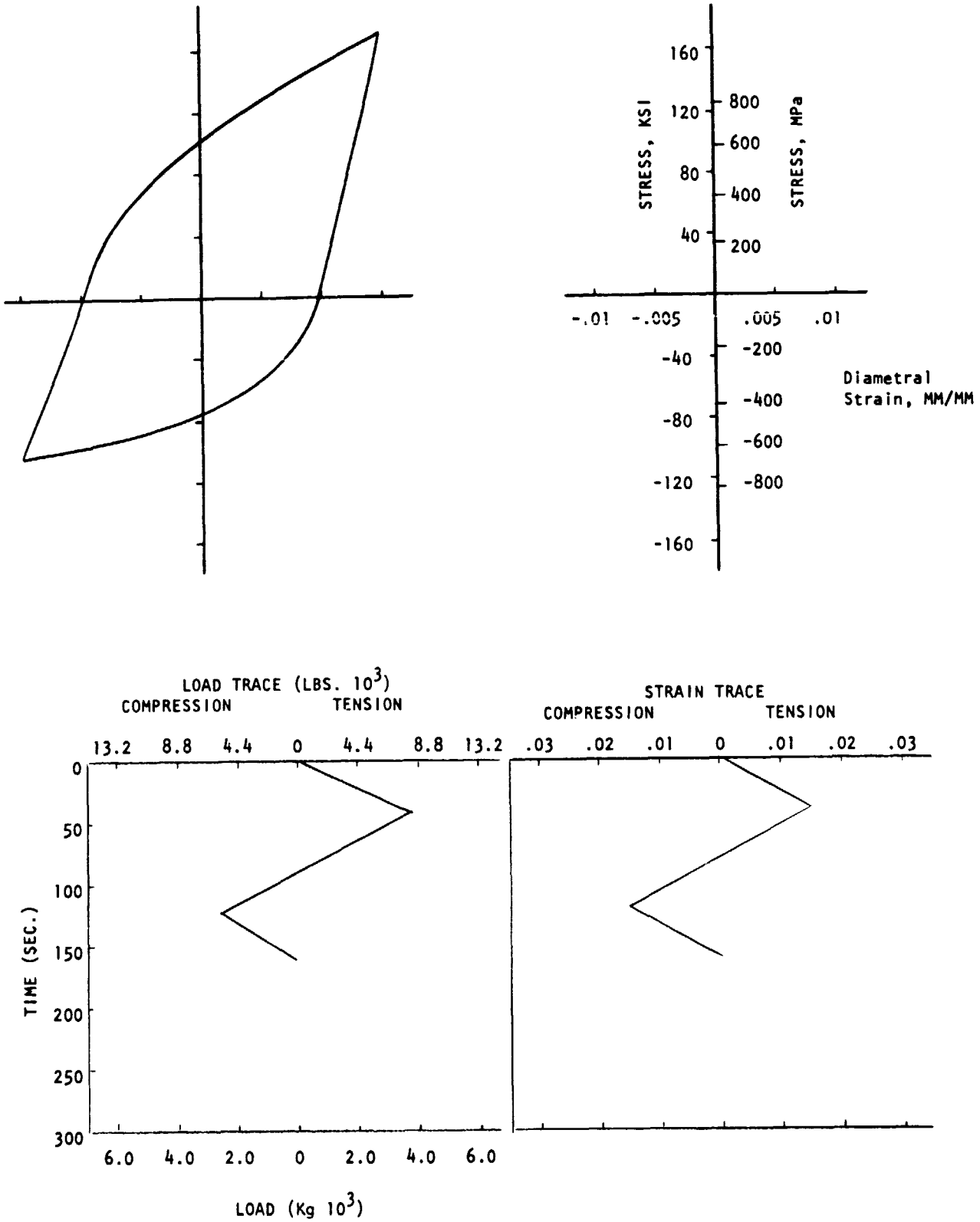

Figure A-12. Hysteresis Loop, Load-Time Trace and Strain Time Trace for A-286, Specimen L62, TCOP Type Test.

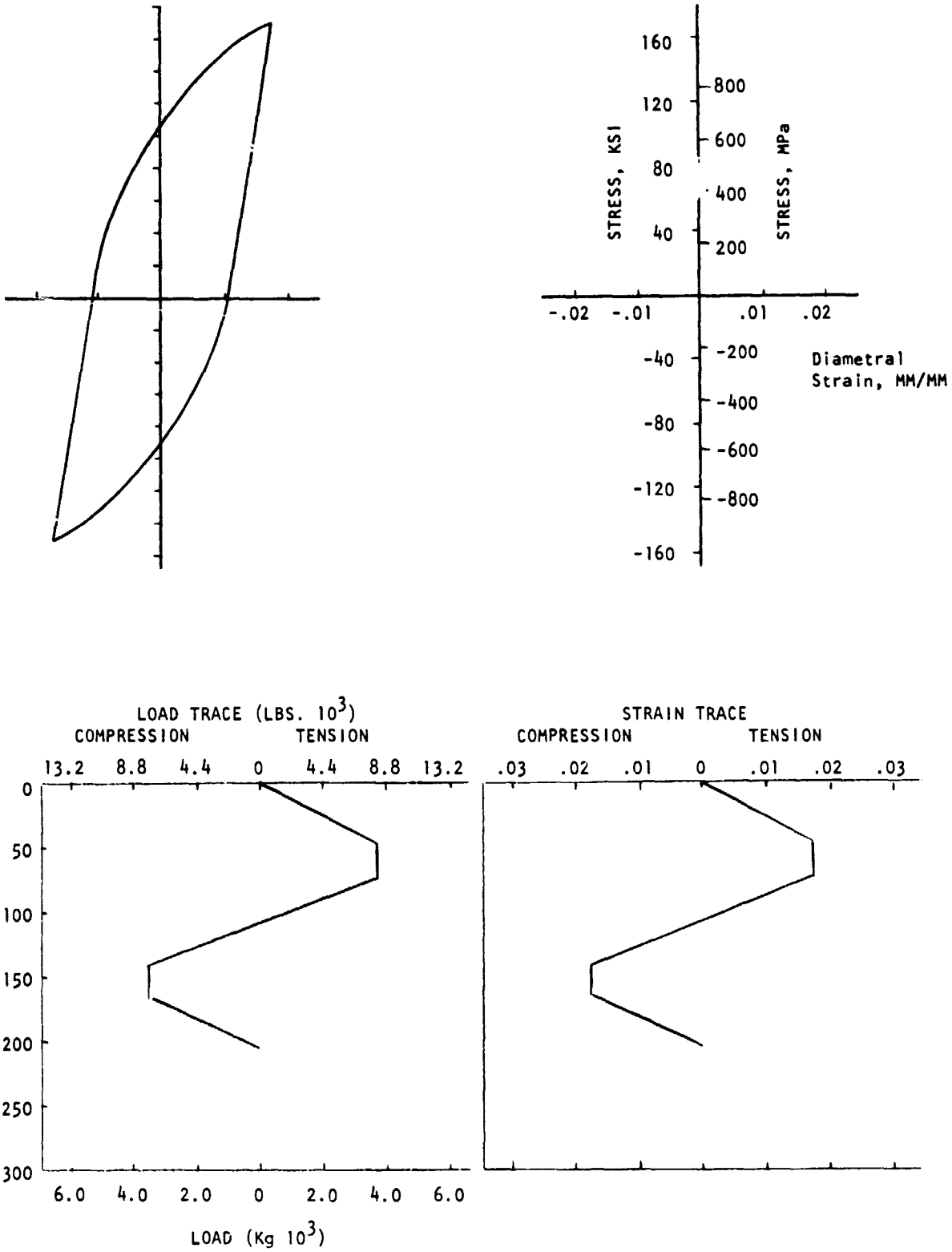

Figure A-13. Hysteresis Loop, Load-Time Trace and Strain Time Trace for A-286, Specimen L58, TCIPS Type Test.

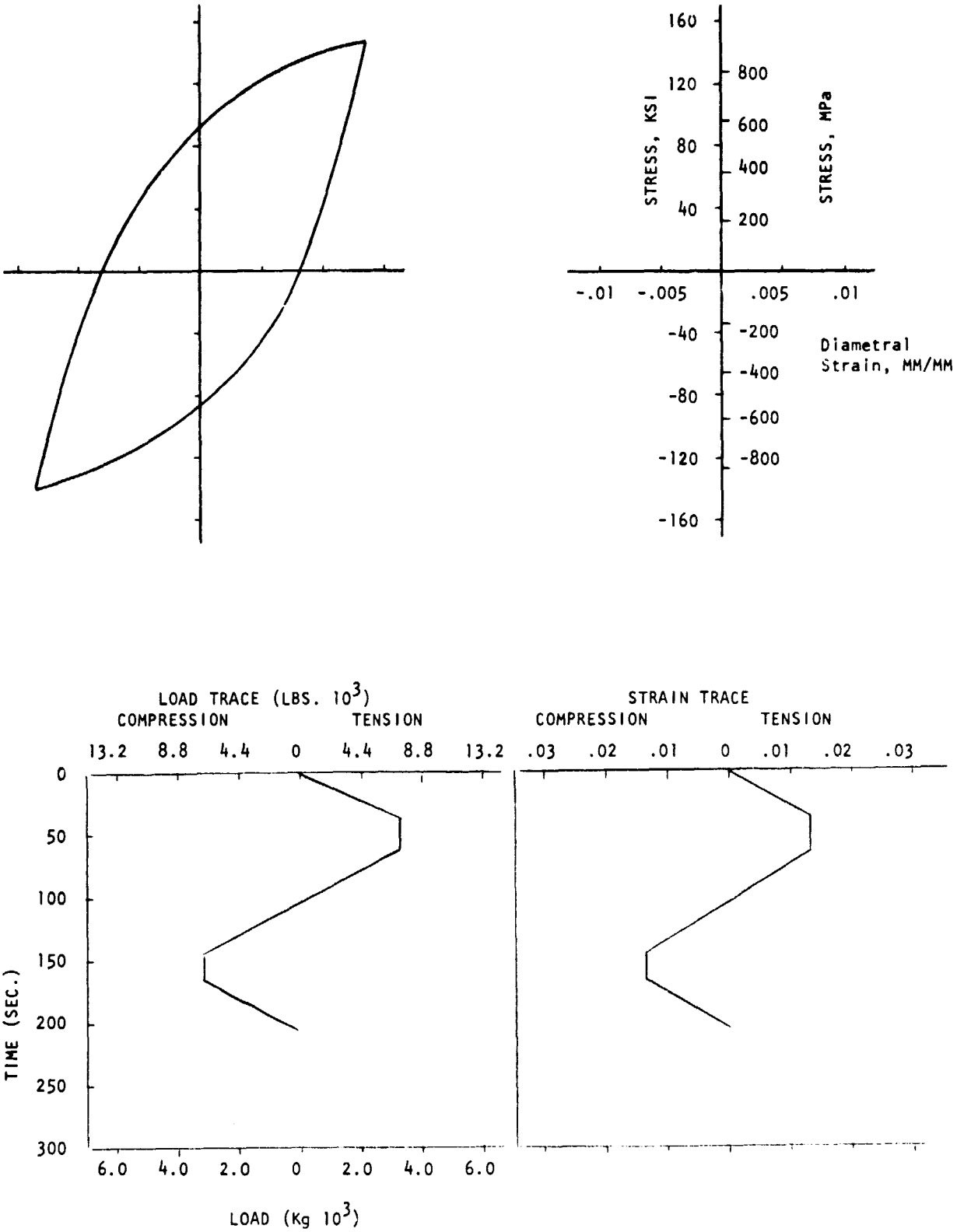

Figure A-14. Hysteresis Loop, Load-Time Trace and Strain Time Trace for A-286, Specimen L59, TCOPS Type Test.